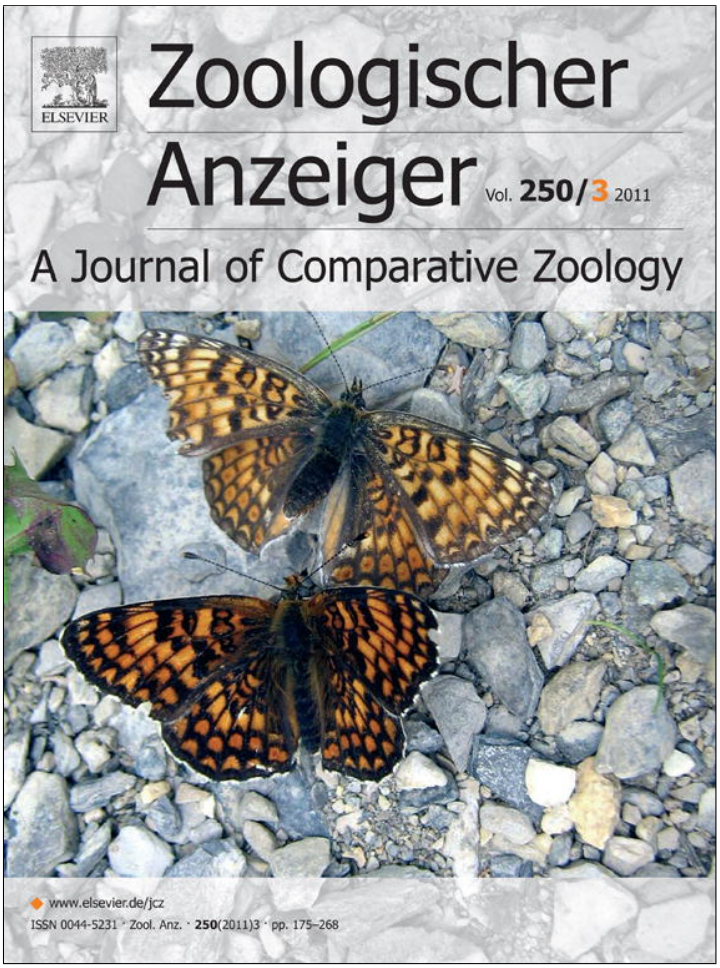

Available online at www.sciencedirect.com
ScienceDirect
Zoologischer Anzeiger 250 (2011) 175–194
Zoologischer Anzeiger
www.elsevier.de/jcz

Geographic distribution and phenetic skull variation in two close species of *Graomys* (Rodentia, Cricetidae, Sigmodontinae)

Juan José Martínez[a,c,*], Valeria Di Cola[b,c]

[a] *Facultad de Ciencias Exactas, Físicas y Naturales, Universidad Nacional de Córdoba, Córdoba, Argentina*
[b] *Laboratorio de Biología del Comportamiento, Facultad de Ciencias Exactas, Físicas y Naturales, Universidad Nacional de Córdoba, Córdoba, Argentina*
[c] *Consejo Nacional de Investigaciones Científicas y Técnicas (CONICET), Argentina*

Received 16 September 2009; received in revised form 3 September 2010; accepted 14 March 2011

Abstract

The interspecific differentiation of South American rodents of the genus *Graomys* was assayed at ecological and morphometric levels in two species. At the ecological level, niche modelling was used. At the morphometric level, the hypothesis that the size and shape of the skull vary with the geographic location was tested using geometric morphometrics by assessing the extent and spatial distribution of phenotypic skull variation within and among two species, *Graomys griseoflavus* and *Graomys chacoensis*. Our results of niche modelling indicate the spatial differentiation between the two species, with *G. chacoensis* inhabiting preferably the Chaco ecoregion and *G. griseoflavus* inhabiting mainly the Monte ecoregion. In multiple linear regressions, approximately 20% of the skull size variation is explained by latitude, altitude, and temperature seasonality. The partial least square analysis reveals strong correlation between shape and environmental variables, mainly with latitude, annual mean temperature, and annual precipitation. Discrimination between *G. griseoflavus* and *G. chacoensis* was highly reliable when using geometric morphometric tools. These results permit us to elucidate some evolutionary processes that have occurred in these species.

Keywords: Geometric morphometrics; *Graomys*; Multivariate analysis; Niche modelling; Phenotypic variation; Environmental correlations; Sigmodontinae

1. Introduction

Ecology plays an important role during the speciation process because evolutionary lineages often occur in different environments or utilize different resources. The adaptation to these different ecological settings drives evolutionary divergence, and the ecological settings can play an additional role in the origin of species (Wiens, 2004). This author pointed out that the species tend to retain similar ecological niches over evolutionary times scales, and the failure to adapt to new environmental conditions is a key factor in initially isolating populations and in creating new lineages. Perhaps the most challenging geographic speciation process to demonstrate is parapatric speciation. When a partly overlapping geographic distribution of two species is observed, it is difficult to determine whether this distribution pattern is due

*Corresponding author at: Facultad de Ciencias Exactas, Físicas y Naturales, Universidad Nacional de Córdoba, Vélez Sarsfield 299 5000, Córdoba, Argentina.
E-mail address: juan_jmart@yahoo.com.ar (J.J. Martínez).

0044-5231/$ – see front matter © 2011 Published by Elsevier GmbH.
doi:10.1016/j.jcz.2011.03.001

to primary contact of species that evolved parapatrically by expanding into a new environment or due to secondary contact of species that evolved allopatrically and extended their ranges to overlap (Coyne and Orr, 2004).

The species of the South American rodent genus *Graomys* (Thomas 1916) provide an excellent system to examine the relationship between ecology and speciation. *Graomys griseoflavus* (Waterhouse 1837) has a wide distribution in the south of South America; from eastern Bolivia and Paraguay south and west of the Paraguayan Chaco to almost all of Argentina. These mice inhabit desert regions, such as the Patagonian steppes, dry forests, savannas, and riparian forests. In general it occurs in regions from sea level to almost 3000 m a.s.l.

Interestingly, high karyotypic variation due to Robertsonian or centric fusion (i.e., whole-arm chromosomal translocation), combined in some individuals with two pericentric inversions, was described mainly in populations from desert regions and the south of Dry Chaco. Among these, two groups were found, namely specimens with $2n = 34$, 35, 36, 37 and 38 and specimens with $2n = 42$ (one specimen from Córdoba province presented $2n = 41$) (Wainberg and Fronza, 1974; Zambelli et al., 1994). A series of studies performed in central-western Argentina confirmed that specimens with $2n = 42$ deserve a taxonomic distinction at the species level, and the name *Graomys centralis* (Thomas, 1902) was employed for these populations (Theiler and Gardenal, 1994; Theiler and Blanco, 1996a,b; Theiler et al., 1999; Catanesi et al., 2002, 2006), confirming the existence of two sibling species. *G. griseoflavus* occurs mainly in the desert ecoregions called the Monte desert and in the Patagonian steppe, and *G. centralis* occurs in the Dry Chaco and Espinal ecoregions (Theiler et al., 1999; Díaz et al., 2006). Ferro and Martínez (2009) suggested, based on molecular and morphometric evidences, that *G. centralis* (Thomas, 1902) must be synonymized under *Graomys chacoensis* (Allen 1901) and concluded that only one species of *Graomys* inhabit the whole Chaco, including the Humid and Dry Chaco and Espinal ecoregions.

Despite the available data about the patterns of genetic variation and differentiation among specimens of *G. griseoflavus* and *G. chacoensis* (=*G. centralis*) from central western Argentina (Theiler et al., 1999; Catanesi et al., 2002, 2006; Martínez et al., 2010b), the geographic distribution and variation in skull shape in *G. chacoensis* and *G. griseoflavus* have never been examined. Martínez et al. (2010a), using traditional morphometrics on specimens collected in central western Argentina, were able to distinguish the two species, but only on the basis of size variation. The main drawback of traditional morphometrics is that it measures size rather than shape and that it can be difficult to separate information about shape from that about size. Fortunately, the geometric morphometrics approach has revolutionized the study of shape change through the use of landmarks and, therefore, presents several advantages over traditional morphometrics (Zelditch et al., 2004).

Recently, there has been an increasing interest in examining geographical shape variation in rodents through the use of advanced geometric morphometric techniques (Fadda and Corti, 2001; Monteiro et al., 2003; Macholán et al., 2008; Colangelo et al., 2010; Piras et al., 2010), as several authors have shown the influence of geography and the environment on phenotypic variation on animals (Asthon et al., 2000; Meiri and Dayan, 2003).

In this study, we examined the interspecific differentiation, spatial distribution using ecological niche modelling, and the phenotypic variation in two South American Sigmodontinae rodents, *G. griseoflavus* and *G. chacoensis*, employing two-dimensional geometric morphometrics of the skull. Additional specimens of *Graomys domorum* (Thomas, 1902) were included for a comparative analysis of phenotypic differentiation. We determined niche differentiation and the morphometric differences between the taxa, examined the existence of a correlation between the geographic distance and the morphometric variation between the taxa, and examined whether there is any environmental factor that correlates with the size and shape variation of the taxa. These analyses will allow us to elucidate the evolutionary processes that have occurred in these species and have generated their distribution patterns.

2. Materials and methods

2.1. Ecological niche modelling

We applied the maximum entropy method, called Maxent (Phillips et al., 2006), which requires only presence records and has been shown to perform well in comparison with other approaches, such as Bioclim and Garp (Elith and Graham, 2006, and references therein), especially at low sample sizes (Hernandez et al., 2006; Pearson et al., 2007). Maxent characterizes probability distributions from incomplete information and is used to estimate the unknown probability distribution defining a distribution of species across the study area. This approach is used to find the probability distribution of maximum entropy (that which is closest to uniform) subject to constraints imposed by the known distribution of the species and environmental conditions across the study area (Phillips et al., 2004; Pearson et al., 2006).

Models were created using the occurrence localities that can be assigned unambiguously to one or the other species by karyotypic and *cyt b* sequence information (Catanesi et al., 2002; D'Elia, 2003; Ferro and Martínez, 2009; Martinez, unpublished). The localities were obtained from the authors' field data and supplemented with museum and literature records (Table 1). In this study, we attempted to minimize the spatial autocorrelation of data by using non-adjacent information. All runs of the program were set with a convergence threshold of 1.0E−5 with 1000 iterations; the regularization value was set to 1.0E−4, and the multiplier was set to 0.75; all runs were set with linear, quadratic and product features.

Table 1. Gazzeteer of localities used for ecological niche modelling.

Localities	Assignation	Latitude	Longitude	Source
chacoensis1	Cyt b	−20.4333	−63.0333	Anderson and Yates (2000)
chacoensis2	Karyotype	−21.9492	−60.4646	Lanzone et al. (2007)
chacoensis3	Cyt b	−25.2000	−59.6333	Ferro and Martínez (2009)
chacoensis4	Cyt b	−25.2167	−59.7000	Ferro and Martínez (2009)
chacoensis5	Cyt b	−27.2001	−63.0333	Martínez et al. (unpublished)
chacoensis6	Cyt b	−29.2576	−59.8426	Martínez et al. (unpublished)
chacoensis7	Karyotype/Cyt b	−28.8838	−66.2846	Lanzone et al. (2007)
chacoensis8	Karyotype/Cyt b	−30.3667	−66.2167	Catanesi et al. (2002)
chacoensis9	Karyotype/Cyt b	−30.6521	−65.9999	Theiler and Gardenal (1994)
chacoensis10	Karyotype	−31.5484	−66.2389	Tiranti (1998)
chacoensis11	Karyotype	−32.2140	−66.6020	García and Walker (2004)
chacoensis12	Karyotype/Cyt b	−29.9147	−63.7763	Theiler (1997)
chacoensis13	Karyotype	−30.4014	−64.3532	Zambelli et al. (1994)
chacoensis14	Karyotype	−30.5445	−65.0143	Tiranti (1998)
chacoensis15	Karyotype	−30.7178	−64.8199	Martínez et al. (2010b)
chacoensis16	Karyotype/Cyt b	−31.3775	−63.9764	Martínez et al. (unpublished)
chacoensis17	Karyotype/Cyt b	−31.3962	−63.4178	Catanesi et al. (2002)
chacoensis18	Karyotype	−31.7865	−63.7775	Zambelli et al. (1994)
griseoflavus1	Karyotype/Cyt b	−27.8350	−66.2854	Suárez et al. (2006) and Martínez et al. (unpublished)
griseoflavus2	Cyt b	−28.1236	−65.7969	Martínez et al. (unpublished)
griseoflavus3	Karyotype	−28.3668	−65.7157	Zambelli et al. (1994)
griseoflavus4	Karyotype	−28.3907	−66.2239	Ramirez et al. (2001)
griseoflavus5	Karyotype	−28.3653	−67.0497	Catanesi et al. (2002)
griseoflavus6	Karyotype	−30.1838	−69.2500	Ramirez et al. (2001)
griseoflavus7	Karyotype	−32.3909	−67.9240	Ramirez et al. (2001)
griseoflavus8	Karyotype/Cyt b	−32.8852	−68.9294	Catanesi et al. (2002)
griseoflavus9	Karyotype/Cyt b	−33.0216	−68.9142	Suárez et al. (2006) and Martínez et al. (unpublished)
griseoflavus10	Karyotype	−33.3201	−68.0812	Suárez et al. (2006) and Martínez et al. (unpublished)
griseoflavus11	Cyt b	−33.4260	−67.5737	Martínez et al. (unpublished)
griseoflavus12	Karyotype/Cyt b	−34.0500	−67.9667	Theiler et al. (1999) and Martínez et al. (unpublished)
griseoflavus13	Karyotype/Cyt b	−34.9998	−67.6753	Suárez et al. (2006) and Martínez et al. (unpublished)
griseoflavus14	Karyotype	−32.7451	−66.7649	García and Walker (2004)
griseoflavus15	Karyotype	−33.3502	−66.6151	García and Walker (2004)
griseoflavus16	Karyotype/Cyt b	−33.7477	−66.6658	García (2003)
griseoflavus17	Karyotype	−32.6914	−65.0023	Martínez et al. (2010b)
griseoflavus18	Cyt b	−32.9604	−65.0433	Martínez et al. (unpublished)
griseoflavus19	Karyotype	−37.5213	−67.5894	Tiranti (1998)
griseoflavus20	Karyotype	−36.6827	−64.3749	Tiranti (1998)
griseoflavus21	Karyotype	−36.8133	−64.4529	Tiranti (1998)
griseoflavus22	Cyt b	−37.9949	−65.6053	Martínez et al. (unpublished)
griseoflavus23	Karyotype	−38.6002	−63.8635	Tiranti (1998)
griseoflavus24	Karyotype	−38.3410	−62.6600	Zambelli et al. (1994)
griseoflavus25	Karyotype	−38.8534	−63.1658	Theiler et al. (1999)
griseoflavus26	Karyotype	−40.8512	−68.1005	Catanesi et al. (2006)
griseoflavus27	Cyt b	−42.4179	−64.0948	D'Elia (2003)
griseoflavus28	Karyotype/Cyt b	−42.7921	−65.0071	Martínez et al. (2010b) and Martínez et al. (unpublished)
griseoflavus29	Karyotype	−28.6642	−66.0642	Pearson and Patton (1976)
griseoflavus30	Karyotype	−28.1063	−67.0904	Pearson and Patton (1976)
griseoflavus31	Karyotype	−28.8463	−66.3495	Pearson and Patton (1976)

Only presence records with information about karyotype or *cyt b* sequences were used.

The variables that were used as predictors were topographic and bioclimatic (Table 2). The topographic variables were the altitude and slope, both derived from the digital elevation model obtained from WorldClim (Hijmans et al., 2005), by applying the ENVI module Topographic Modelling. The bioclimatic factors used were data on 19 climatic variables, obtained from WorldClim (Hijmans et al., 2005). Such composites of climatic and topographic data from WorldClim (Hijmans et al., 2005) have been shown to be effective data inputs for large-scale predictions of species

Table 2. Environmental variables used to model the geographic distribution of *Graomys griseoflavus* and *G. chacoensis* in South America.

Environmental variables
BIO1 = Annual mean temperature[a,c]
BIO2 = Mean monthly temperature range[a,c]
BIO3 = Isothermality (BIO2/BIO7 × 100)[a]
BIO4 = Temperature seasonality (STD × 100)[a,c]
BIO5 = Max temperature of warmest month[a,c]
BIO6 = Min temperature of coldest month[a]
BIO7 = Temperature annual range (BIO5 − BIO6)[a]
BIO8 = Mean temperature wettest quarter[a]
BIO9 = Mean temperature driest quarter[a,c]
BIO10 = Mean temperature warmest quarter[a]
BIO11 = Mean temperature coldest quarter[a]
BIO12 = Annual precipitation[a,c]
BIO13 = Precipitation wettest month[a]
BIO14 = Precipitation driest month[a,c]
BIO15 = Precipitation seasonality (CV)[a,c]
BIO16 = Precipitation wettest quarter[a]
BIO17 = Precipitation driest quarter[a]
BIO18 = Precipitation warmest quarter[a]
BIO19 = Precipitation coldest quarter[a]
Altitude[b,c]
Slope[b,c]

[a] Hijmans et al. (2005).
[b] From the digital elevation model obtained from WorldClim (Hijmans et al., 2005), by applying the ENVI module Topographic Modelling.
[c] Variables selected for niche modelling.

distributions (Di Cola et al., 2008). In short, a total of 21 environmental variables were considered and all variables have a post-processing pixel size of 8 km × 8 km. From these 21 variables, before running the models, we selected only 10 environmental variables in order to not over-parameterize our niche models with redundant climatic information (Table 2). A series of correlation tests were conducted to remove redundant variables. The environmental information was extracted from the same localities used for the ecological niche modelling, and a Pearson correlation coefficient of 0.75 was used to identify highly correlated variables. For pairs of variables that were highly correlated, we chose the variable that we considered to be biologically more meaningful and easier to interpret (Rissler et al., 2006; Rissler and Apodaca, 2007).

Binary maps that predicted presence or absence were created from the Maxent-generated niche-based distribution models using the lowest presence threshold value (LPT; see Pearson et al., 2006; Stockman and Bond, 2007). The LPT is determined by selecting the lowest predicted value for the set of presence points used to generate the geographic distributional models. The synthetic maps for each species were obtained in the software ENVI 4.5 (ITT Visual Information Solutions).

Principal components analyses (PCA) in PAST (Hammer et al., 2001) were conducted over the correlation matrix with the values extracted for each environmental layer of presence localities to examine the overall levels of divergence in the ecological niche. A *t*-test was used over the two principal PC axes to determine whether separation in the ecological niche was statistically significant.

Subsequently, we determined the degree and significance of distribution models overlap between the species using the procedure outlined in Stockman and Bond (2007), which employs a Monte Carlo algorithm, which was implemented in the computer program D-NOVL v1.3 (Stockman et al., 2008), to generate the probability distribution of the extent of overlap expected for the observed distribution models. The degree of overlap was calculated as the ratio of the area of overlap to the area of the smaller of the two ranges (Barraclough and Vogler, 2000). The overlap values may range from 0 to 1; where 1 indicates that the species with the smaller range is completely contained within the larger one. 100 simulations were performed with the island method, one island per species. This method allows to select the number desired of growth areas (i.e., islands) and later to estimate the overlap area between species [for details about this method see Stockman et al. (2008)]. The null hypothesis that distributional models are randomly distributed is rejected if the observed range overlap has a probability of <0.05.

2.2. Geometric morphometrics

A total of 185 skull specimens of 52 localities (Fig. 1) from the Colección Mamíferos Lillo (Universidad Nacional de Tucumán, Tucumán, Argentina), Colección de Mamíferos de la Universidad Nacional de Río Cuarto (Universidad Nacional de Río Cuarto, Río Cuarto, Argentina), and the personal collection of Gerardo R. Theiler (Universidad Nacional de Córdoba, Córdoba, Argentina) were examined to elucidate the shape differences among the three species [*G. griseoflavus* ($N = 62$), *G. chacoensis* ($N = 119$), and *G. domorum* ($N = 4$)]. The specimens of *G. domorum* included in our study belong to *G. domorum lockwoodi sensu* Díaz (1999) and Díaz and Barquez (2007). Detailed information about the voucher specimens is provided in Appendices A and B.

A total of 185 dorsal and 177 ventral views of skulls of adult individuals [M3 erupted, age classes 2–5 following Myers (1989)] were examined. To these, *G. griseoflavus* contributed 62 dorsal and ventral views, *G. chacoensis* 119 dorsal views and 111 ventral views, and *G. domorum* 4 dorsal and ventral views.

The images of skulls were taken by one of the authors (JJM) using a digital camera. In order to reduce distortion artefacts due to parallaxis, the specimens were positioned at the centre of the field of view, and the horizontal position of skulls was checked visually prior to the taking of the photographs. For pictures taken of the dorsal side of the skull, the incisors and the tympanic bullae touched the horizontal supporting surface; whereas for pictures taken of the ventral side, the frontal bones touched the horizon-

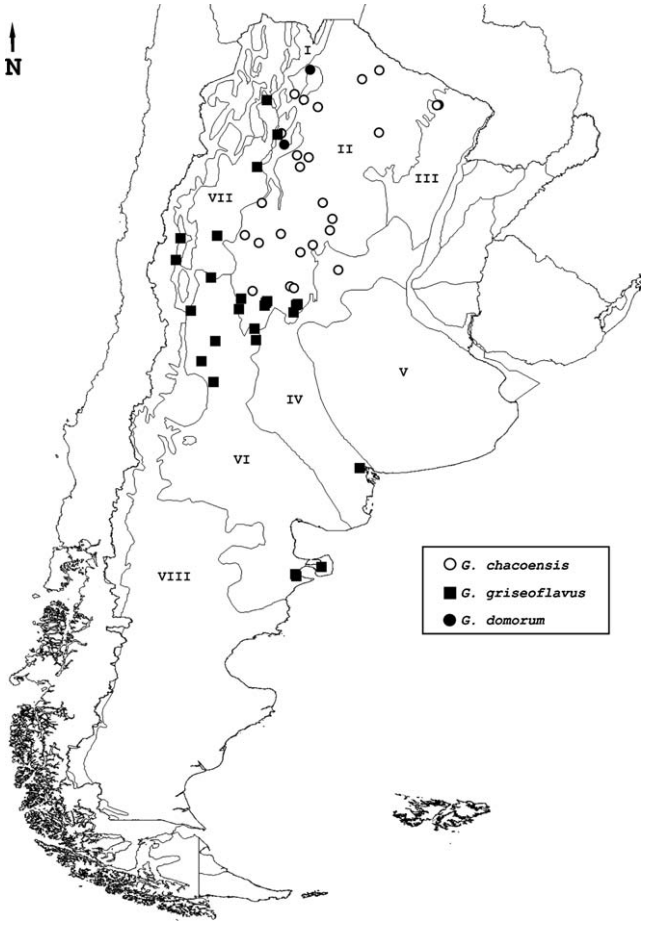

Fig. 1. Map with localities from which specimens of *Graomys* spp. were collected (for details, see Appendix B). Symbols: black squares = localities of *G. domorum*; black dots = localities of *G. griseoflavus*; open circles = localities of *G. chacoensis*. Boarders of countries are indicated by thick lines. Ecoregions, where *Graomys* spp. occur, are delimited by thin lines: I = "Yungas", of cloud rain forest; II = "Dry Chaco", xerophytic forest; III = "Humid Chaco", xerophytic forest mixed with palm savannas; IV = "Espinal", *Prosopis* spp. (Fabaceae, Fabales) trees forest; V = "Pampa", grassy prairie and grass steppe; VI = "Monte of prairie and plateau regions", shrub steppe of prairie and plateau regions; VII = "Monte of mountain regions", shrub steppe of mountain regions and VIII = "Patagonian steppe", cold and dry shrub steppe.

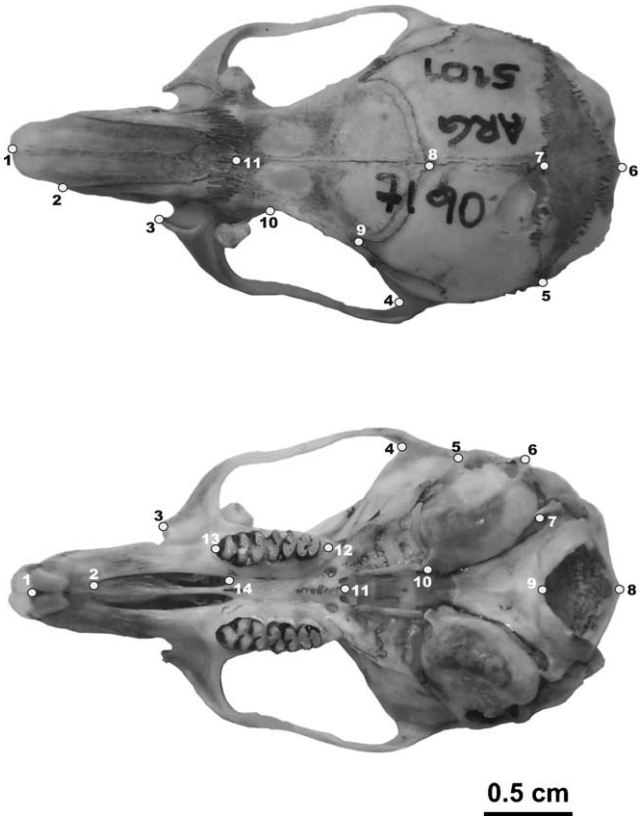

Fig. 2. Landmarks captured for this study on dorsal and ventral views of a skull (*G. chacoensis* CML7190, 26 km to south-west of Quimilo, La Rioja province). Dorsal view of skull: 1 = rostralmost point of the nasal bone; 2 = intersection of the rostral curvature of the nasal process of the incisive and the nasal bones in a dorsal projection; 3 = rostral end of zygomatic plate; 4 = caudalmost point of orbit; 5 = intersection of the parietal–interparietal and interparietal–occipital sutures; 6 = caudal end of the curvature of the occipital bone; 7 = intersection of the sagittal and parietal-interparietal sutures; 8 = intersection of the coronal and sagittal sutures; 9 = rostralmost point of the parietal bone; 10 = narrowest point of the interorbital region; 11 = intersection of the naso-frontal suture in the midline. Ventral view of skull: 1 = rostralmost point of the upper incisor tooth next to the midline; 2 = rostral end of the rostral palatine fissure; 3 = rostral end of the zygomatic plate; 4 = caudalmost point of the orbit; 5 = rostral end of the external opening of the bony portion of the auditory canal; 6 = caudal end of the external opening of the bony auditory canal; 7 = caudalmost point of the intersection between the tympanic bulla and jugular foramen; 8 = caudal end of the occipital foramen in the midline; 9 = rostral end of the occipital foramen in the midline; 10 = centralmost point of the Eustachian tube; 11 = caudalmost point of the suture between palatine bones and the rostral border of the mesopterygoid fossa; 12 = caudalmost point of the molar row; 13 = rostralmost point of the molar row; 14 = caudal end of the palatine fissure.

tal supporting surface. Landmarks were digitized by JJM on one side of the skull to minimize potential influence of any asymmetry.

Eleven landmarks were digitized on the dorsal side of the skulls and 14 on the ventral side with the TpsDig2 program (Rohlf, 2005a) (see Fig. 2). The registered points correspond to landmarks of type 1 (anatomical juxtaposition of tissues) and type 2 (points of maximum curvature or other morphogenetic processes) (Bookstein, 1991). The error due to the operator (measurement error) was checked by one-way ANOVA of centroid size, which were taken three times on different occasions from 25% of the specimens selected randomly. The measurement errors were very low: 0.004% for the dorsal views and 0.008% for the ventral views.

All configurations of landmarks were superimposed using the least-squared method of generalized Procrustes

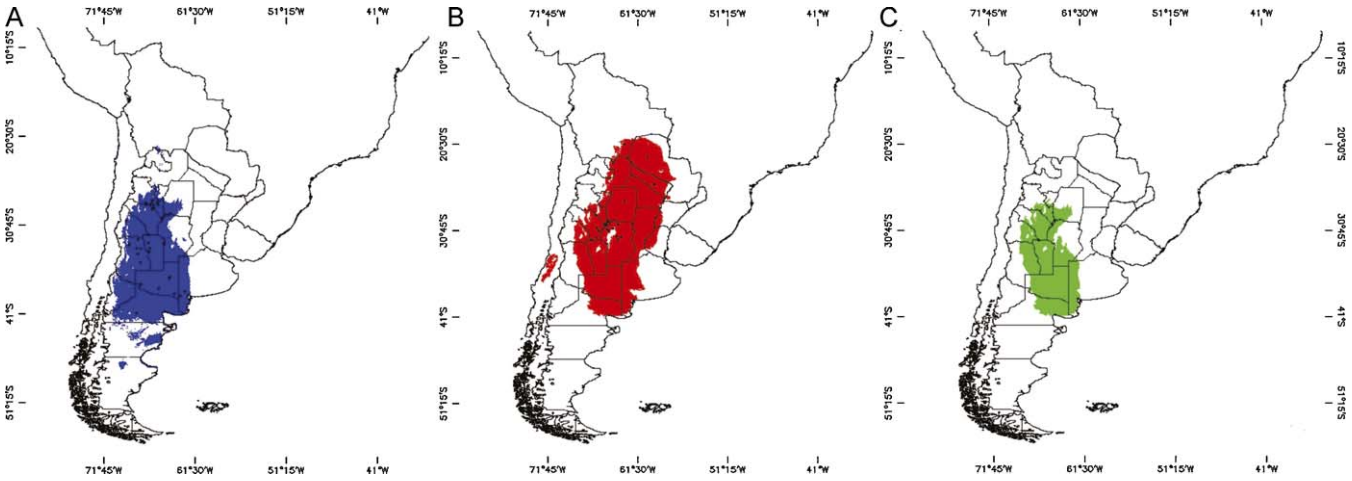

Fig. 3. Maps of probability areas for the occurrence of *Graomys griseoflavus* and *G. chacoensis* according to the Maximum Entropy models, predicting with high probability the presence of species in South America at 8 km × 8 km scale. (A) *G. griseoflavus*. (B) *G. chacoensis*. (C) Area of probable overlap between *G. griseoflavus* and *G. chacoensis*.

analysis (GPA) (Rohlf and Slice, 1990) implemented in TpsRelw (Rohlf, 2005d). The software TpsSmall (Rohlf, 2005e) was used to calculate the relationships between Procrustes and Euclidean distances.

Shape variations were described through aligned Procrustes coordinates and partial warps for each specimen. The size of the skull was expressed as the centroid size and computed as the square root of the sum of squared distances between each landmark and the configuration centroid. Interspecific shape differences were examined with Canonical Variables Analysis (CVA) using aligned Procrustes coordinates as input. Shape changes associated with the variation along canonical axes were visualized through deformation grids by regressing the partial warp scores on the canonical scores using the TpsRegr program (Rohlf, 2005c). The rates of correct classification based on *a priori* group assignments were obtained by comparing these ones with the classification based on CVA-distance-based method using CVAGen of IMP series (Sheets, 2001a), which determines the probability that the specimen is closer to the mean of the group to which it was assigned *a priori* than to the mean of another group (Zelditch et al., 2004). Size differences among species were assessed with an ANOVA implemented in PAST (Hammer et al., 2001).

The allometric component was tested by multivariate regression of the weight matrix (shape variation) following Macholán et al. (2008) and González-José et al. (2008) as function of centroid size using IMP Regress6 program (Sheets, 2001b). The dorsal and ventral images of 171 specimens were used for a partial least square (PLS) analysis to explore patterns of shape covariation between the dorsal and ventral sides as described by Rohlf and Corti (2000) and to determine any covariation between the relative positions of landmarks on the dorsal and ventral projections of the skull.

The degree of correlation between geographic and morphometric distances (Procrustes distance) within species was examined by the Mantel test (Mantel, 1967) with 5000 permutations using the PAST program (Hammer et al., 2001). The geographic distances between localities were obtained using GenAlEx (Peakall and Smouse, 2006).

PLS analyses (Rohlf and Corti, 2000), implemented in TpsPLS (Rohlf, 2005b), were carried out to test whether the shape differences are related to different environmental factors. This technique allowed the determination of any relationships between the two sets of variables (e.g., shape, represented by partial warps plus uniform component, and environmental variables). PLS constructs pairs of vectors representing linear combinations of the variables within each set. These linear combinations are such that the vectors account for as much of the covariation between the two original sets of variables as possible. The new variables describe the patterns, if any, of covariation between the two sets of original variables. Additionally, the sizes of skulls (dorsal and ventral centroid sizes) were regressed with the same environmental variables in order to determine changes in size along the climatic and geographic gradients. We performed multiple regressions with InfoStat (2008).

The environmental predictors used for this analysis were latitudinal, longitudinal, topographic, vegetational and bioclimatic variables. The topographic variables were altitude and slope, which were derived from the digital elevation model obtained from WorldClim (Hijmans et al., 2005) by applying the ENVI module Topographic Modelling. The vegetation variables used were the Mean Normalized Difference Vegetation Index (NDVI) and NDVI Standard Deviation. NDVI was measured by the advanced very high resolution radiometer (AVHRR), which is on board of the National Oceanic and Atmospheric Administration's (NOAA) polar-orbiting meteorological satellites. NDVI data are monthly averaged products derived from satellite images from the 1982 to 2000 period. The climatic factors used were data on six climatic variables [i.e., annual mean

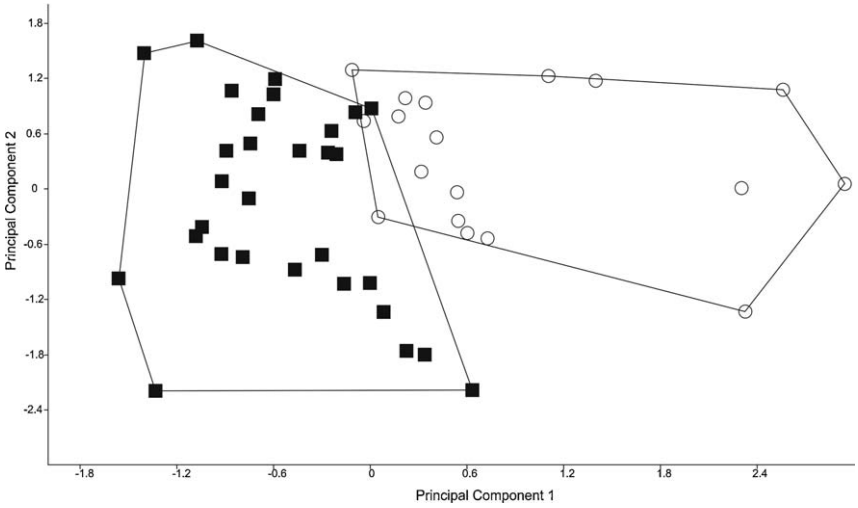

Fig. 4. Principal components analysis of occurrence records showing niche differentiation between *G. griseoflavus* and *G. chacoensis*. The first principal component explains 40.08% of the variation, and the second one explains 25.52%. Total variation explained by the first two principal components is 65.5%. Symbols: black squares = *G. griseoflavus*; open circles = *G. chacoensis*.

temperature, temperature seasonality (standard deviation of monthly temperature), minimum temperature of coldest month, maximum temperature of hottest month, annual precipitation, precipitation seasonality (standard deviation of monthly precipitation)] obtained from WorldClim (Hijmans et al., 2005).

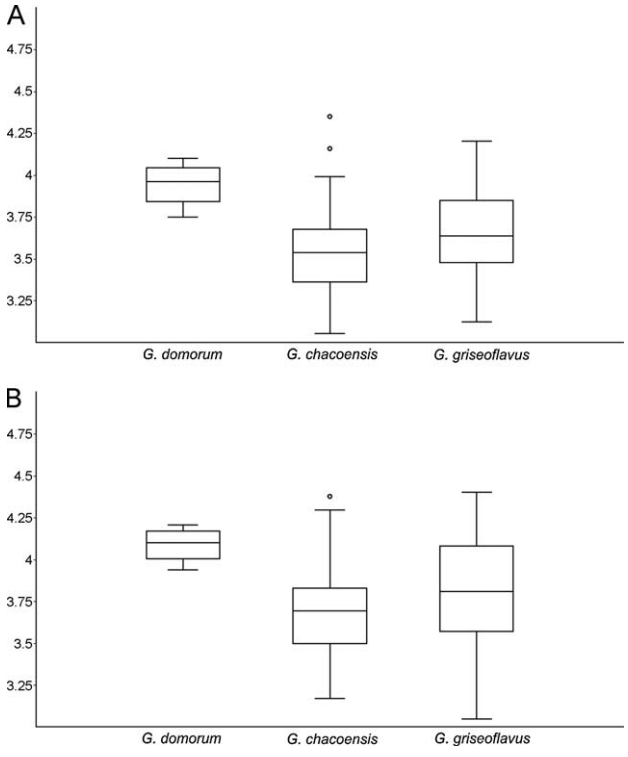

Fig. 5. Box plots showing skull size variability between *Graomys* spp. The box plots present medians, 25 and 75 percentiles; limits are the 95% confidence intervals. Outliers are represented as black dots. (A) Dorsal views of the skulls. (B) Ventral views of the skulls.

3. Results

3.1. Geographic distribution and niche differentiation

Niche models for *G. chacoensis* and *G. griseoflavus* and their areas of probable overlap are shown in Fig. 3. The overlap ranges are high (0.6082), and the probability that these ranges are randomly distributed is <0.05. The distributional models of each species indicate that *G. chacoensis* predominantly inhabit the Chaco ecoregion and that *G. griseoflavus* occur preferentially in the Monte ecoregion. The PCA (Fig. 4) and the *t*-test performed over the PC scores (PC1: $t = 6.693$, $p < 0.001$; PC2: $t = 1.8$, $p = 0.078$) show that these two species occupy statistically significantly different niches. Principal component loadings show that positive values of PC1 are related to annual mean temperature, mean temperature of driest quarter, and annual precipitation. In contrast, negative values of PC1 are related to altitude, slope, mean monthly temperature range, and temperature seasonality. Positive values of the PC2 are related to annual mean temperature, maximum temperature of warmest month, and precipitation seasonality. Finally, precipitation of the driest month is the main variable that accounts for negative values. The distributional models show that the contact zones of the ranges appear to be suitable for both species (Fig. 3).

3.2. Interspecific size differences

The ANOVA on centroid size reveal significant differences among species ($F = 10.49$, $df = 2$, $p < 0.001$; $N = 185$) on the dorsal centroid size and ($F = 8.445$, $df = 2$, $p < 0.001$; $N = 177$) on the ventral centroid size. We found significant differences in centroid sizes between *G. domorum* and the other two species, in particular with *G. chacoensis* ($p < 0.001$

and $p < 0.01$ for the dorsal and ventral sides, respectively) being smaller than *G. domorum*. The size differences between *G. domorum* and *G. griseoflavus* were significant only for the dorsal side of skull ($p < 0.05$), but not for the ventral side ($p = 0.057$). *G. domorum* tends to have larger skulls than *G. griseoflavus*. The size differences between the skulls of *G. chacoensis* and *G. griseoflavus* were not significant ($p > 0.05$), although *G. griseoflavus* specimens tend to have larger skulls (Fig. 5).

3.3. Interspecific shape differences

The correlations between Procrustes (Kendall shape space) and Euclidean (tangent space) distances in the dorsal and ventral configurations were almost 1, suggesting an almost perfect approximation of shape space through the tangent space.

The canonical variables analysis (CVA) based on landmarks on the ventral side of the skull discriminate better between species than that based on landmarks on the dorsal side of the skull (Fig. 6). Table 3 shows the rates of correct classification of the dorsal and ventral views of the skull. In general, the rates were high, always exceeding 75% of correct classification (75.63–100% for the dorsal view of the skull, and 79.28–100% for the ventral view).

In the dorsal view of the skull, *G. domorum* is separated from *G. griseoflavus* and *G. chacoensis* along the second axis (Fig. 6A) on the basis of enlarged nasals, the major distance between landmarks 7–8, and the major distance between landmarks 4–9. Overall, the specimens of *G. domorum* have a more robust braincase and greater orbital arches than the other two species (Fig. 7). *G. chacoensis* and *G. griseoflavus* are separated along the first axis. The main difference is found at landmarks 7 and 8: *G. griseoflavus* has a longer distance between these landmarks than *G. chacoensis*. At the most rostral point of the parietal bone in *G. chacoensis*, the landmark 4 is near the caudal maximum curvature of the zygomatic process of the temporal bone (Fig. 7).

The CVA based on landmarks on the ventral side of the skull is shown in Fig. 6B. *G. domorum* is more differentiated than the other two species along the axes 1 and 2 as it has a smaller tympanic bulla. In *G. domorum*, the maxillary tooth row (landmarks 12 and 13) is shorter than that in the other two species. In *G. domorum*, the caudal tip of the incisive foramen ends before the beginning of the maxillary tooth row in contrast to *G. chacoensis* and *G. griseoflavus* whose caudal tips of the incisive foramina extend slightly beyond the apical edge of the first upper molar (M1) (Fig. 7). *G. griseoflavus* and *G. chacoensis* are differentiated mainly along axis 1: In *G. griseoflavus*, the tympanic bulla is well developed, the distance between landmarks 8–9 is shorter than that in *G. chacoensis*, and the incisive foramen is slightly shorter than that in *G. chacoensis* (landmarks 2 and 14). *G. griseoflavus* specimens have a more caudally located mesopterygoid fossa than *G. chacoensis*, and *G. chacoensis* specimens have a more caudally divergent caudal maximum curvature of the zygomatic process of the temporal bone than *G. griseoflavus* (Fig. 7). Allometry was not significant after 1000 permutations of Wilk's Lambda parameter (Wilk's Lambda: 0.1843, $p = 0.565$, $N = 185$ for the dorsal view of the skull, and Wilk's Lambda: 0.1841, $p = 0.642$, $N = 177$ for the ventral view).

The PLS analysis of dorsal and ventral covariation based on 171 specimens reveals that the first pair of vectors explain 90.81% of total covariance ($p < 0.001$), and that these vectors are highly correlated ($r = 0.806$, $p < 0.001$). The bivariate plot for the first pair of vector is shown in Fig. 8, which also depicts what shape aspects of the two sides of the skull covary. At negative values, the more apparent aspects that covary include a broader braincase (i.e., expanding shifts of dorsal landmarks 4, 6, 8 and 9), enlarged and broad tympanic bullas (i.e., expanding shift of ventral landmarks 5, 6 and 10), and an enlarged foramen magnum (i.e., increasing distance between ventral landmarks 8 and 9). There is also covariation among reduced nasals (i.e., decreasing distance between dorsal landmarks 1 and 11), narrowest interorbital breadth (i.e., retracting shift of dorsal landmark 10), and reduced diastema length (i.e., decreasing distance between ventral landmarks 1 and 13). At positive values, the relationships among landmarks are reversed (Fig. 8).

3.4. Environmental correlates of skull size and shape variation

The variance analysis on multiple linear regressions of the dorsal and ventral centroid sizes and the 12 environmental variables is reported in Tables 4 and 5, respectively. The environmental variables explain 17% ($F = 4.03$, $df = 12$, $p < 0.0001$) of the skull size variation in the dorsal view. Similarly, the environmental variables explain 19% ($F = 4.14$, $df = 12$, $p < 0.0001$) of the ventral centroid size variation. The only four variables with significant effects comprise latitude, altitude, temperature seasonality, and minimum temperature of the coldest month. The skull size tends to decrease with an increase in latitude and altitude, and tends to increase with an increase in temperature seasonality and the minimum temperature of the coldest month.

In general, the correlations between geographic and Procrustes distances were not significant within species [i.e., dorsal view of *G. chacoensis* (Mantel test: $R = 0.046$, $p = 0.311$); ventral view of *G. chacoensis* (Mantel test: $R = 0.019$, $p = 0.429$); ventral view of *G. griseoflavus* (Mantel test: $R = 0.163$, $p = 0.109$)], except for the dorsal view of *G. griseoflavus*, whose correlation was significant (Mantel test: $R = 0.216$, $p = 0.024$).

The PLS analysis indicates a relationship between the dorsal shape of the skull and the environmental variables. The first pair of vectors explain 58.72% of the total covariation ($p > 0.05$) and were correlated ($r = 0.343$, $p < 0.05$). The shape vector was correlated mainly with NDVI ($r = 0.325$), NDVI SD ($r = 0.321$), annual

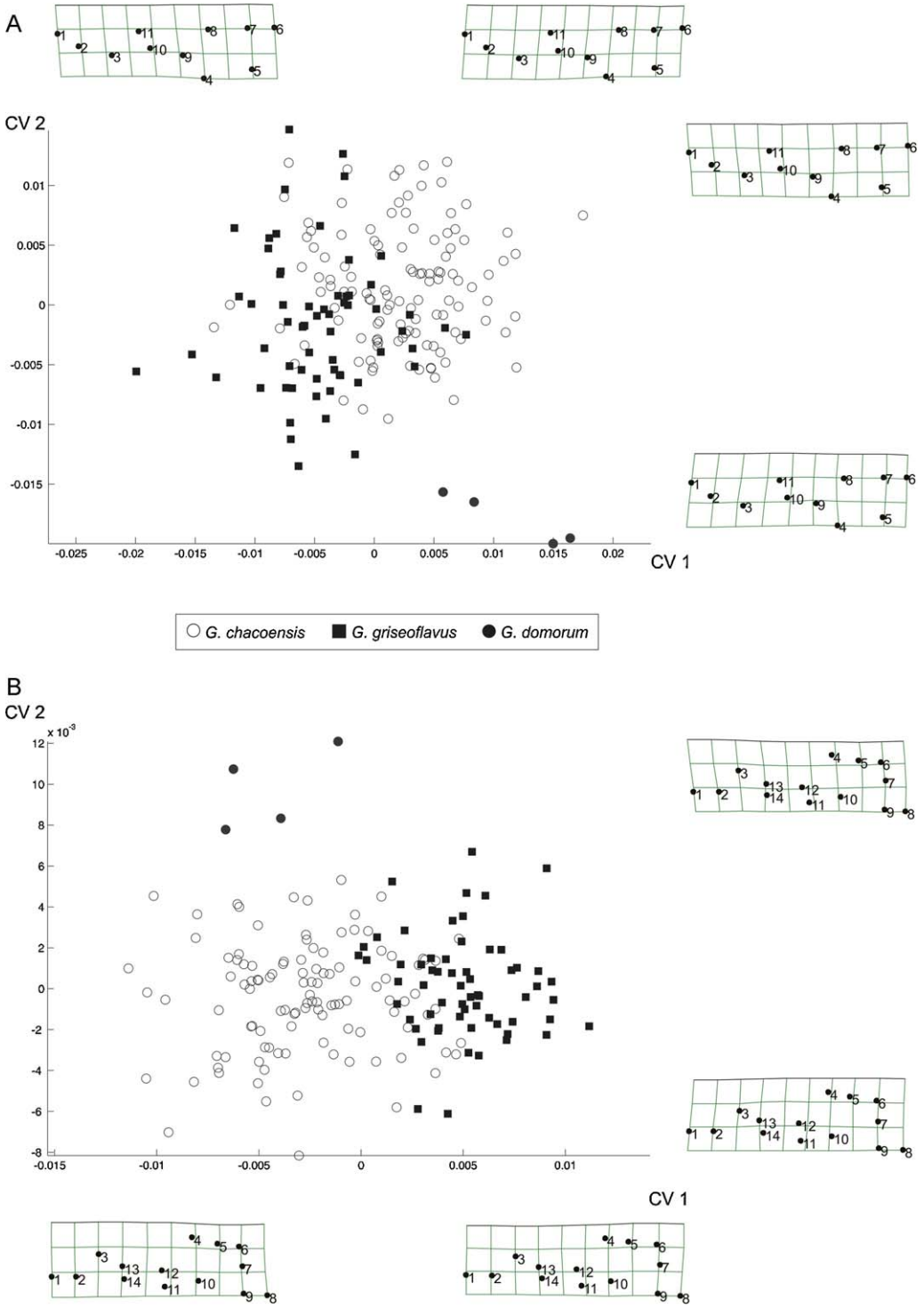

Fig. 6. Canonical variation analyses (CVA) of Procrustes coordinates of the skull showing species differentiation. Deformation grids of thin-plate splines for extremes for each axis are depicted. (A) Dorsal view of the skulls. (B) Ventral view of the skulls. Symbols: black dots = *G. domorum*; open circles = *G. chacoensis*; black squares = *G. griseoflavus*.

precipitation ($r = 0.293$), and longitude ($r = 0.29$). At negative values of the first shape vector, skulls show correlations among decreased nasals (i.e., decreasing distance between dorsal landmarks 1 and 11), narrowest interorbital breadth (i.e., retracting shift of dorsal landmark 10), more rostrally positioned intersection of the coronal and sagittal sutures (i.e., dorsal landmark 8), and expanding braincase (i.e., expanding shift of dorsal landmarks 4 and 5) (Fig. 9). At positive values of the shape vector skull shapes were reversed.

Table 3. Classification results of the CVA by species.

Original group	Predicted group membership			%
	G. domorum	*G. chacoensis*	*G. griseoflavus*	
Dorsal view of skull				
G. domorum $N=4$	4	0	0	100
G. chacoensis $N=119$	0	90	29	75.63
G. griseoflavus $N=62$	0	14	48	77.42
Ventral view of skull				
G. domorum $N=4$	4	0	0	100
G. chacoensis $N=111$	2	88	21	79.28
G. griseoflavus $N=62$	0	4	58	93.55

% is the percent of correctly classified individuals.

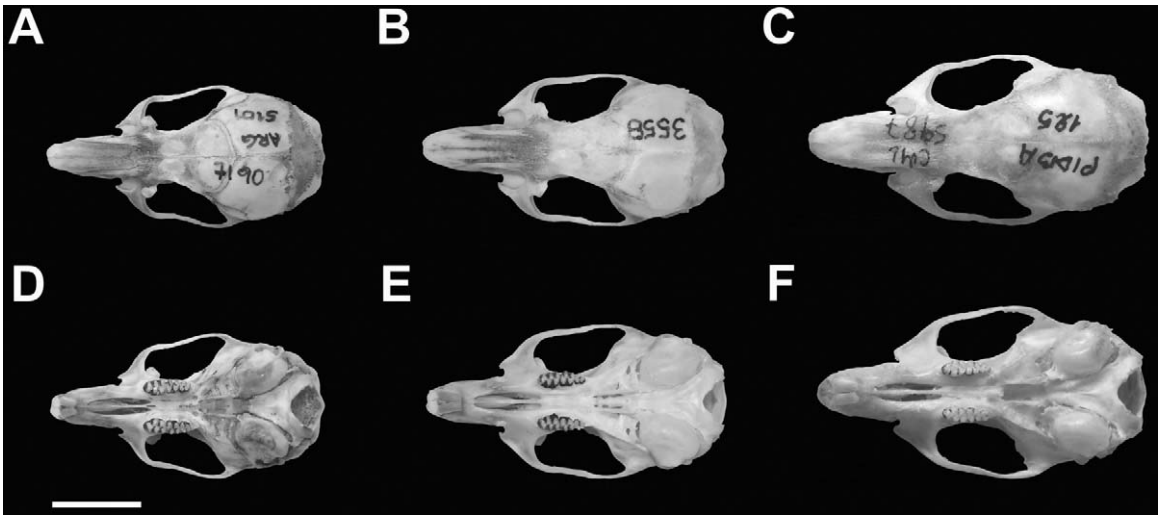

Fig. 7. Photographs of dorsal (A–C) and ventral views (D–F) of skulls of *Graomys* spp. (A and D) *G. chacoensis* CML7190, 26 km to south-west of Quimilo, La Rioja province. (B and E) *G. griseoflavus* CML3538, Puesto Punta del Agua, Mendoza province. (C and F) *G. domorum* CML5987, Las Tipas, Parque Biológico San Javier, Tucumán province. The skull of *D. domorum* skull is larger with a more robust braincase. The main difference between *G. chacoensis* and *G. griseoflavus* is the tympanic bulla, which is larger in *G. griseoflavus*. Scale: 1 cm.

Table 4. Regression of dorsal centroid size onto geoclimatical variables; regression coefficients, standard errors (SE) and *t*-test of significance of predictors.

Variables	Coefficients	SE	*t*	Probability
Latitude	0.11	0.04	3.09	0.0023
Longitude	0.05	0.03	1.80	0.0731
Altitude	−5.7E−04	2.7E−04	−2.11	0.0359
Slope	0.04	0.02	1.65	0.1000
Annual mean temperature	−0.02	0.01	−1.80	0.0736
Temperature seasonality	6.5E−04	1.6E−04	4.08	0.0001
Max temperature of warmest month	0.01	0.02	0.94	0.3507
Max temperature of warmest month^2	−3.9E−05	2.8E−05	−1.42	0.1580
Min temperature of coldest month	0.01	5.0E−03	2.91	0.0041
Annual precipitation	−2.4E−04	2.2E−04	−1.06	0.2893
Precipitation seasonality	−2.2E−03	3.1E−03	−0.73	0.4691
NDVI	−2.5E−03	2.3E−03	−1.06	0.2885
NDVI SD	0.01	0.01	1.04	0.3004

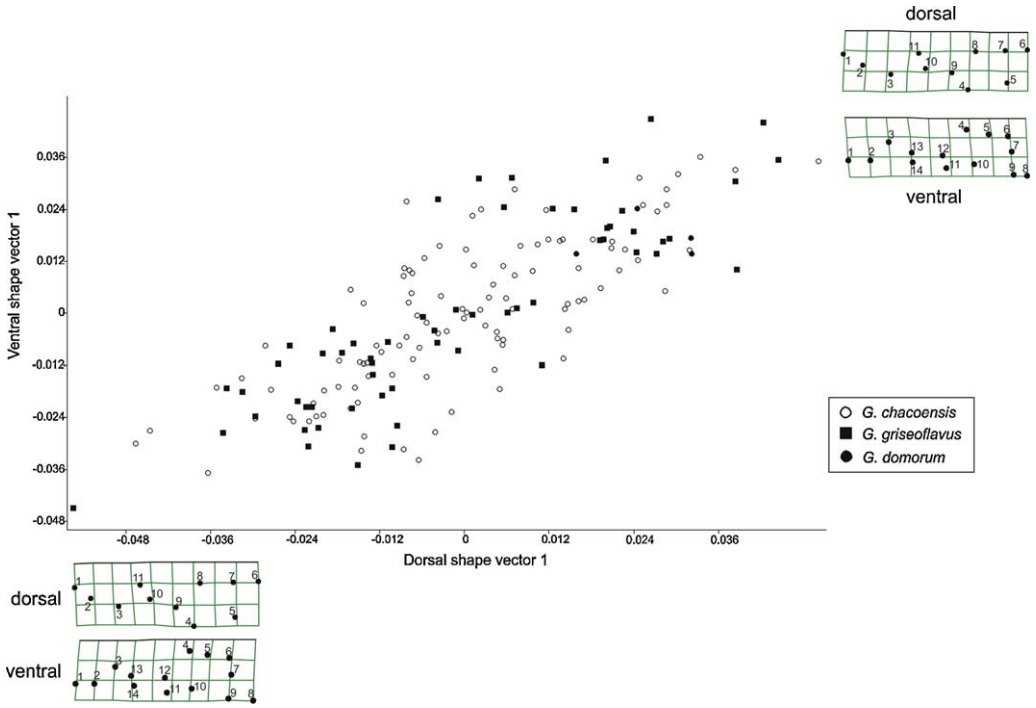

Fig. 8. Partial least square analysis results (PLS) of the skull shapes in the dorsal and ventral views of the *Graomys* spp. The correlation between the first pair of vectors of maximum covariation is shown. The abscissa of the scatterplot represents the shape changes in the dorsal view (dorsal shape vector 1), and the ordinate represents shape changes in the ventral view (ventral shape vector 1). Deformation grids for the negative and positive ends of the shape vectors are shown. Symbols: open circles = *G. chacoensis*, black squares = *G. griseoflavus*; black dots = *G. domorum.*

The second pair of vectors, representing 32.07% of the total covariation (with a marginal significance $p = 0.05$) and 98.70% of the cumulative covariation ($p < 0.05$) were significantly correlated ($r = 0.42$, $p = 0.002$). In particular, the shape of the skull was correlated with latitude ($r = 0.32$) and precipitation seasonality ($r = 0.35$) (Fig. 9). At negative values of the second shape vector, the skull presents enlarged nasals due to an expanding shift of dorsal landmark 1, retracting shifts of dorsal landmarks 4 and 9 resulting in expanding zygomatic arches, and decreasing distance between landmarks 6 and 7, principally due to a retracting shift of landmark 6 (Fig. 9). At positive values of the second shape vector, the skull aspects were reversed.

A strong relationship between the shape in the ventral view of the skulls (but not in the dorsal view), and biogeophysical variables was found. The first pair of vectors, which explained 79.17% of the total covariation ($p = 0.039$), were highly correlated ($r = 0.74$, $p = 0.001$). This positive correlation involves

Table 5. Regression of ventral centroid size onto geoclimatical variables: regression coefficients, standard errors (SE) and *t*-test of significance of predictors.

Variables	Coefficients	SE	*t*	Probability
Latitude	0.15	0.04	3.38	0.0009
Longitude	0.06	0.03	2.15	0.0328
Altitude	−6.9E−04	3.1E−04	−2.21	0.0285
Slope	0.04	0.03	1.51	0.1319
Annual mean temperature	−0.03	0.01	−1.91	0.0574
Temperature seasonality	8.6E−04	1.8E−04	4.66	<0.0001
Max temperature of warmest month	0.02	0.02	1.26	0.2101
Max temperature of warmest month^2	−5.7E−05	3.1E−05	−1.85	0.0659
Min temperature of coldest month	0.02	0.01	3.48	0.0006
Annual precipitation	−4.4E−04	2.6E−04	−1.71	0.0894
Precipitation seasonality	−2.7E−03	3.5E−03	−0.77	0.4405
NDVI	−3.4E−03	2.6E−03	−1.29	0.2002
NDVI SD	0.01	0.01	1.21	0.2296

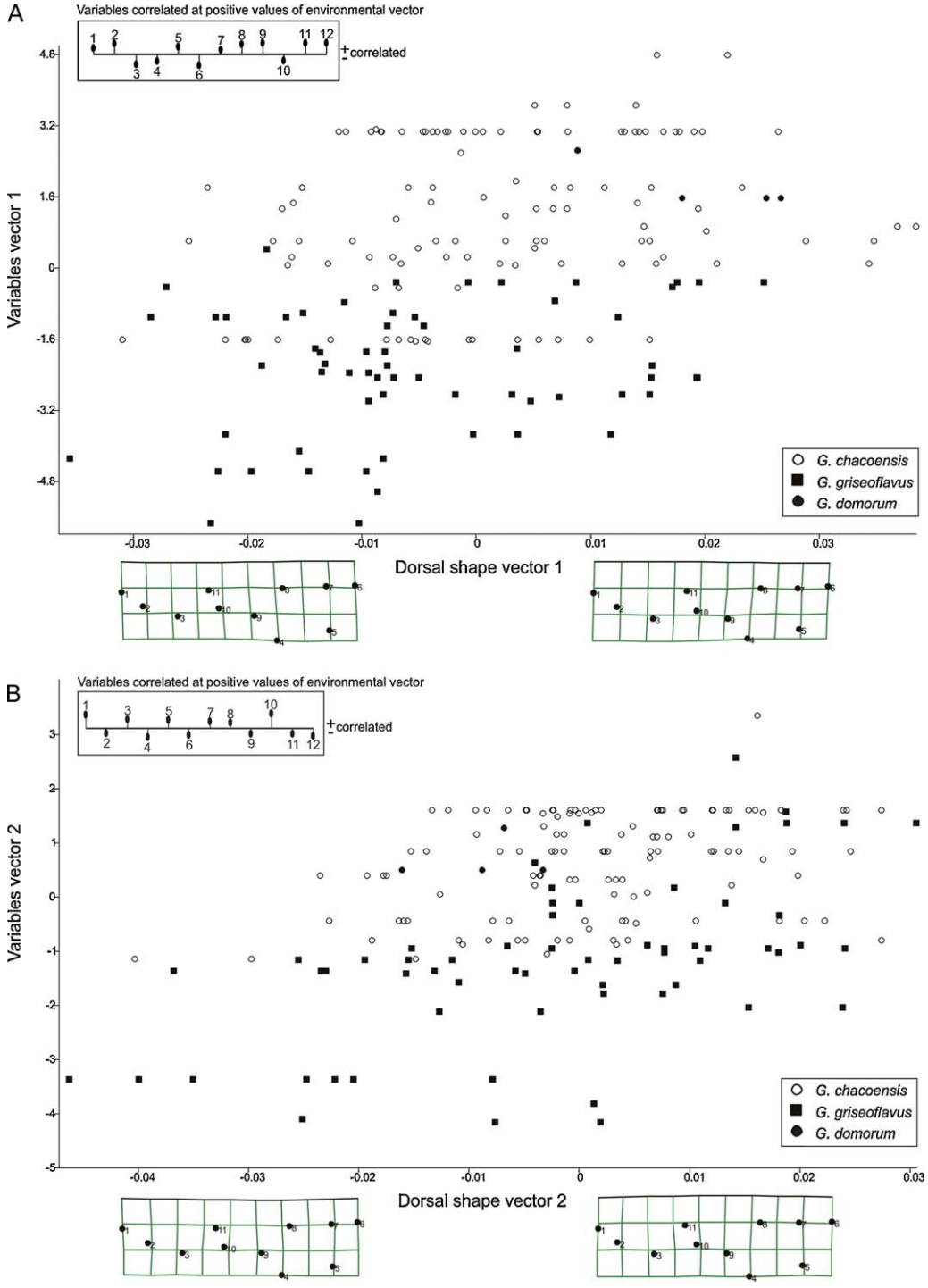

Fig. 9. Partial least square analysis results (PLS) of the shape variables in the dorsal view of the skulls and geoclimatic variables. The correlations between the two first vectors of maximum covariation are shown. Abscissas of the scatterplots represent the shape changes (shape vectors) and ordinates represent the geoclimatic changes (variables vectors), and they are explained by the respective boxes at the positive end of the axes. Deformation grids for the negative and positive ends of the shape vector are shown. For positive values of variables vectors, the positive or negative correlations of each geoclimatic variable are shown. The vertical sticks above and below the horizontal line represent positive and negative correlations, respectively. (A) Scatterplot of dorsal shape vector 1 and geoclimatic vector 1. (B) Scatterplot of dorsal shape vector 2 and geoclimatic vector 2. Symbols: open circles = *G. chacoensis*; black squares = *G. griseoflavus*; black dots = *G. domorum*. Geoclimatic variables: 1 = latitude, 2 = longitude, 3 = altitude, 4 = slope, 5 = annual mean temperature, 6 = temperature seasonality, 7 = minimum temperature of coldest month, 8 = maximum temperature of hottest month, 9 = annual precipitation, 10 = precipitation seasonality, 11 = NDVI and 12 = NDVI SD.

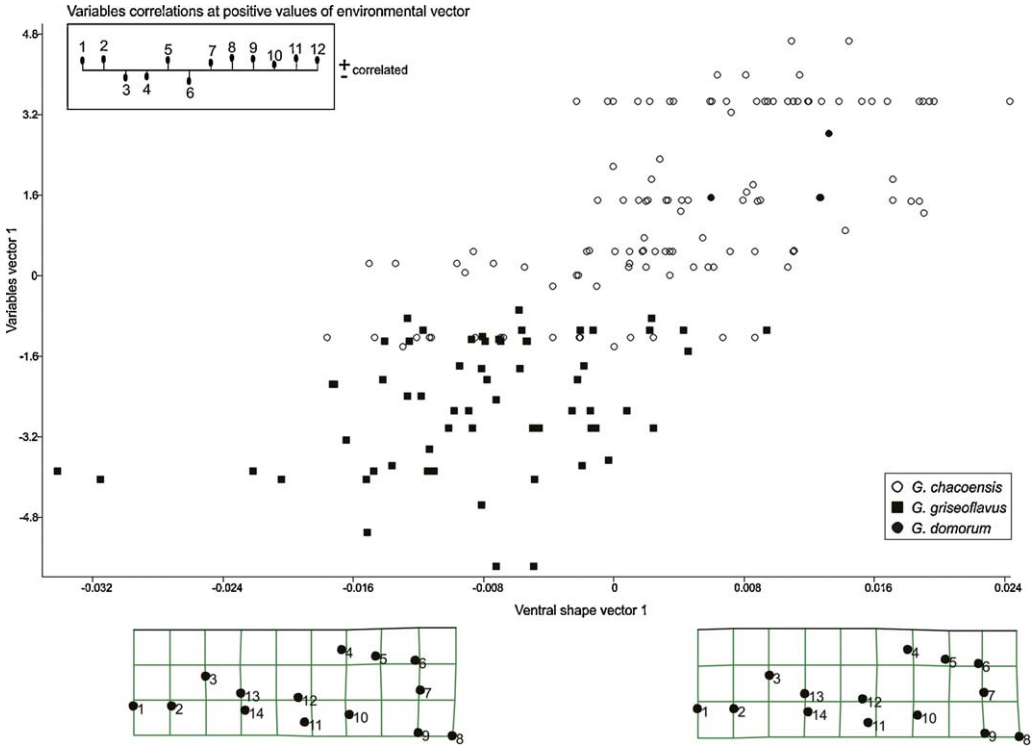

Fig. 10. Partial least square analysis results (PLS) of shape variables of the ventral view of the skulls and geoclimatic variables. The correlation between the first pair of vectors of maximum covariation is shown. The abscissa of the scatterplot represents the shape changes (shape vector 1), and the ordinate represents the geoclimatic changes (variables vector 1), and they are explained by the box at the positive end of the axis. Deformation grids for the negative and positive ends of the shape vector are shown. For positive values of the variable vector, positive or negative correlations of each geoclimatic variable are shown. The vertical sticks above and below the horizontal line represent positive and negative correlations, respectively. Symbols: open circles = *G. chacoensis*; black squares = *G. griseoflavus*; black dots = *G. domorum*. Geoclimatic variables: 1 = latitude, 2 = longitude, 3 = altitude, 4 = slope, 5 = annual mean temperature, 6 = temperature seasonality, 7 = minimum temperature of coldest month, 8 = maximum temperature of hottest month, 9 = annual precipitation, 10 = precipitation seasonality, 11 = NDVI and 12 = NDVI SD.

the skull shape on the one hand and, on the other hand, latitude ($r = 0.55$), longitude ($r = 0.63$), annual mean temperature ($r = 0.56$), minimum temperature of coldest month ($r = 0.69$), and annual precipitation ($r = 0.60$), NDVI ($r = 0.64$). In contrast, the skull shape is negatively correlated with temperature seasonality ($r = -0.65$) (Fig. 10). At negative values, the main morphological character associated with the first shape vector is an enlargement of the tympanic bulla due to expanding shifts of landmarks 5, 6, 7 and 10 (Fig. 10). At positive values of the first vector, there is a reversed trend with a decrease of the tympanic bulla.

4. Discussion

4.1. Interspecific differences at ecological and phenotypic levels

This is the first study that provides evidence for a correlation between the variation of skull shape and ecogeographical variables in a sigmodontine rodent, in particular in *G. griseoflavus* and *G. chacoensis*. Our study also found evidence for niche differentiation between *G. griseoflavus* and *G. chacoensis*. We did not include the fundamental niche estimation for *G. domorum* because the taxonomic status of its synonyms has not yet been resolved.

The incorporation of GIS-based tools in evolutionary studies has revolutionized the understanding of ecology in the origin of species (Kozak et al., 2008). Our niche modelling results show the spatial differentiation between *G. chacoensis*, which preferably inhabits the Chaco ecoregion, and *G. griseoflavus*, which inhabits mainly the Monte ecoregion (Fig. 3). The distribution of *G. chacoensis* is related to high annual mean temperatures and precipitations. The distribution of *G. griseoflavus* is positively correlated with altitude, slope, and temperature seasonality. The overlap area between the two species is wider than expected. This distribution pattern may imply an ecological interchangeability between the two species, which may eventually lead to a hybridization of the species. However, Theiler (1997) and Theiler et al. (1999) did not find any evidence for hybridization or introgression based on karyotypes or allozyme variation in areas of proximity between the two species. The geographical overlap could be explained in light of the range limits that may be set by interactions with other species of the same genus or from species belonging to other genera, rather than by climatic conditions. Moreover, Tiranti (1998) showed that in ecotonal

zones, *G. griseoflavus* occurs in the Espinal ecoregion or in marginal areas of the Chaco ecoregion. This fact may be the reason for the great area of overlap revealed by our ecological niche modelling.

The interspecific differences in centroid size in the dorsal and ventral views of the skulls are consistent in that *G. domorum* has a larger skull than the other two species, and that *G. griseoflavus* tends to have a larger skull than *G. chacoensis*. These results agree with those of traditional morphometrics by Martínez et al. (2010a), which find significant differences between *G. griseoflavus* and *G. chacoensis* in fourteen of the nineteen measurements used. These measurements were larger in *G. griseoflavus* than in *G. chacoensis*.

The data from the ventral view of the skulls allow a better discrimination between the species than the data from the dorsal view. But the analysis of both data sets reveals that *G. domorum* is more divergent from the other two species than these are from each other. In general, *G. domorum* has a robust braincase, less well developed tympanic bullae [see also Thomas (1902, 1926) and Anderson (1997)], larger orbital arches, smaller maxillary tooth rows, and incisive foramina that end rostrally to the maxillary tooth row. In contrast, *G. griseoflavus* possesses well developed tympanic bullae, and smaller incisive foramina than *G. chacoensis*, which has a more rostrally positioned *fossa mesopterygoidea* than *G. griseoflavus*. Some of these results are very similar to and corroborate the ones found by Martínez et al. (2010a) using traditional morphometrics. These results can be used for the taxonomic identification of specimens and as a basis for future morphological analyses of the genus *Graomys*.

Allometry was not found at the size variation examined [ages 2–5 defined by Myers (1989)]. Hingst-Zaher et al. (2000), who studied the variation in postnatal changes in skull size and shape in *Calomys expulsus* (Sigmodontinae, Phyllotini), found that most variation in skull shape occurs before 20 days of age. Future studies will be needed to establish whether a similar pattern of postnatal shape variation occurs in *Graomys* species.

The PLS analysis of the two views of the skull reveals a high covariation. However, the taxonomic information, such as the ecophenotypic information, is not the same for the two views. The discrimination power is better in the ventral side of the skull (see Table 3 and Fig. 6), which is supported by other studies showing that different skull structures provide dissimilar phylogenetic information (i.e., Lockwood et al., 2004; Macholán, 2008). Different selective constraints on the various parts of the skull are probably responsible for these differences. It would be worthwhile to compare the phylogenetic signal of skull shape in Sigmodontinae taxa.

4.2. Environmental correlates of phenotypic variation

The size of the skulls varies in a clinal manner. The centroid size decreases with geoclimatic variables, mainly from north to south, and with altitude. Accordingly, the size of the skulls increases with temperature seasonality. The maximum temperature of the warmest month is not correlated with the variation of the centroid size variation, but the increase of the minimum temperature of the coldest month (from temperatures below 0–10 °C) have a significant positive effect on the size of the skull. The size of the skull was not correlated with productivity variables, such as precipitation and NDVI, in contrast to Cardini et al. (2007), who found that higher rainfall is correlated to larger skulls in males of Vervet monkeys (*Cercopithecus aethiops*, Primates). The absence of a relationship between rainfall and size may be because temperature is a more significant climate driver in the region where *Graomys* species occur. Another possibility is that rainfall as a proxy for productivity does not apply to small mammals in the same manner as it does to large mammals. This issue will need to be analyzed more deeply with other large and small mammal species in South America.

Size and shape variation patterns of the skull can also be discussed in the context of the currently known phylogeny of the species by considering the different environments that characterize the geographical range of the genus (Fadda and Corti, 2001). The range of *Graomys* in Argentina encompasses different phytogeographic regions or ecoregions: Yungas cloud forest, Dry and Humid Chaco savannah forest, Espinal forest, Monte desert of hilly and prairie regions, and Patagonian steppe (Díaz et al., 2006). Theiler et al. (1999) pointed out that *G. griseoflavus* specimens were found mainly in the Monte desert and the Patagonian steppe regions, although some marginal populations were found in the Espinal forest region according to Tiranti (1998). *G. chacoensis* (=*G. centralis*) specimens were found in Espinal and Western Chaco forests (Theiler et al., 1999), although, as mentioned above, Ferro and Martínez (2009) proposed that specimens from the northern part of Argentina, the Bolivian Chaco, and Paraguay belong to the same species as those from central-western Argentina and showed that this species inhabits dry and humid Chaco and Espinal forests. Díaz et al. (2006) and Díaz and Barquez (2007) showed that *G. domorum* specimens occur in Yungas cloud forest, in the Prepuna regions, and in the ecotonal regions of the Dry Chaco and Yungas.

In general, the populations studied were not isolated by geographical distance. This result corroborates the results of genetic studies (Theiler et al., 1999; Catanesi et al., 2002, 2006; Martínez et al., 2010b). However, a correlation between morphometrics and geographic distance was observed ($p < 0.05$) when the features of the dorsal side of the skull of the *G. griseoflavus* were considered separately by locality. Already earlier, Theiler et al. (1999) were unable to find a correlation between the number of effective migrants (Nm) and the geographic distance between populations and pointed out that a recent and rapid colonization could be responsible for this distribution pattern. Subsequently, Martínez et al. (2010b) did not find a correlation between the phylogenetic relationships of mtDNA

haplotypes and the geographic distribution. In addition, the analyses to determine geographic expansion [i.e., mismatch distribution (Rogers and Harpending, 1992) and Fu neutrality test (Fu, 1997)] confirmed that both species experienced bursts of geographical expansion.

Partial least square analyses demonstrate that morphometric variation reflects the different environments in which the various species of *Graomys* occur, albeit to a different degree for the dorsal and ventral views of the skull. For example, in the dorsal view of the skull of *G. griseoflavus*, the shape of the skull was not strongly correlated with environment variables (see Fig. 9). In contrast, there was a strong correlation between the shape of the tympanic bulla and the geoclimatic variables, as it is correlated positively mainly with latitude ($r = 0.55$), longitude ($r = 0.63$), annual mean temperature ($r = 0.56$), minimum temperature of the coldest month ($r = 0.69$), annual precipitation ($r = 0.60$) and NDVI ($r = 0.64$), and is negatively correlated with temperature seasonality ($r = -0.65$). A functional interpretation of these differences is not easy, but other authors (Taylor et al., 2004) pointed out that enlarged tympanic bullae in South African rodents of the tribe Otomyni (Muridae) is an adaptation to arid and open habitats, enhancing thereby the sense of hearing for predator-avoidance. The pioneering works of Webster on rodents of the Family Heteromyidae in North America suggest that the enlargement of the middle-ear bony structures is related to a more acute sensitivity to low frequency sounds (Webster, 1962, 1966; Webster and Webster, 1980). Our results confirm that *G. griseoflavus*, which inhabit open and arid habitats, tend to have larger tympanic bullae than species inhabiting forest and savannas habitats. Further studies are needed in order to interpret this morphological change as an adaptive outcome.

The phenotypic evolution of the skull in rodents is the product of a variety of evolutionary forces (i.e., natural selection, genetic drift, etc.), and the phylogenetic history may not be the predominant factor (Fadda and Corti, 2001). In this study, it could be shown that the geoclimatic variation does not correlate with the shape of the skull equally in the dorsal and ventral views, indicating perhaps that different cranial structures are subject to different selective pressures. This issue deserves further study to gain insight into the adaptive significance of the geographic variation of cranial morphology. The close relationship between the shape of the ventral side of the skull and the geoclimatic variables is, in part, explained by an adaptation to local climate conditions (see above). Therefore, molecular or cytogenetics techniques may need to be employed in addition to morphological and morphometric methods to define species boundaries in this complex group of sigmodontine rodents.

Acknowledgements

We are grateful to L. Ignacio Ferro and Rubén Barquez (Universidad Nacional de Tucumán), José Priotto and Jaime Polop (Universidad Nacional de Río Cuarto) and Gerardo Theiler (Universidad Nacional de Córdoba) for kindly providing the specimens used in this study. We thank our respective advisors, C. Noemí Gardenal and Margarita Chiaraviglio, for infrastructural support. We also are grateful to Dominique G. Homberger and two anonymous reviewers, whose comments and suggestions greatly improved this work. JJM and VD are fellows of the Consejo Nacional de Investigaciones Científicas y Técnicas (CONICET) and doctoral students of the Doctorado de Ciencias Biológicas, Universidad Nacional de Córdoba.

Appendix A.

List of examined specimens of *Graomys* species, their geographical origin, and their accession or catalogue number. The acronyms of the museums and collections are as follows: CML = Colección Mamíferos Lillo, Universidad Nacional de Tucumán, Tucumán; CUNRC = Colección de Mamíferos, Universidad Nacional de Río Cuarto, Río Cuarto; and GRT = the personal collection of Gerardo R. Theiler, Universidad Nacional de Córdoba, Córdoba. "d" or "v" indicates that a specimens was used for analyses of the dorsal or ventral views of the skull.

G. domorum lockwoodi: Argentina. Jujuy province, Laguna La Brea (CML5985 d v); Tucumán province, Las Tipas Parque Biológico San Javier (CML5986 – 5988 d v).

G. chacoensis: Argentina. Catamarca province, Chumbicha (CML3477 – CML3478 d v, CML3481 d v, CML3483 – CML3484 d v); Córdoba province, 10 km N of Santiago Temple (GRT035 d v), Cruz del Eje (GRT031 – GRT034 d v, GRT040 d v, CUNRC2178 d, CUNRC2180 d v, CUNRC2195 d v, CUNRC4264 d v, CUNRC4952 – CUNRC4954 d v, CUNRC44781 d v), Deán Funes (GRT037 – GRT039 d v), Villa de María (GRT029 – GRT030 d v, CUNRC1523 d v, CUNRC1526 d v, CUNRC4004 – CUNRC4006 d v, CUNRC4047 v, CUNRC4052 d v, CUNRC4066 d v, CUNRC4137 d v), Villa Dolores (CUNRC50103 d v), Yacanto (CUNRC2387 d v, CUNRC2816 d v); Formosa province, Cruce entre ruta 81 and 95 7 km N (LIF078 d v), Estancia Poguazú, Cruce entre ruta 81 and 95 8 km N (LIF118 d v), 35 km S, 5 km E Ingeniero Guillermo Juarez, Puesto Divisadero (CML3572 v, CML3934 – CML3935 d v, CML3972 d,); La Rioja province, 26 km SW Quimilo (CML7189 – CML7191 d v), Chamical (CUNRCcha10 d v, CUNRCcha20 d v, GRT024 – GRT026 d v, GRT027 d, GRT028 d v), Guayapa, Patquía (CML1392 d, CML1393 d v, CML1514 – CML1515 d, CML1516 – CML1519 d v, CML1521 – CML1525 d v, CML1566 d, CML1567 d v, CML1569 d v, CML1570 d, CML1574 d, CML1598 d v); Salta province, 32 km NE of La Lumbrera (CML6028 d v), Cabeza de Buey (CML357 d v, CML464 d v, CML668 d, CML671 d v, CML911 d v), 19 km SE of Joaquín V. González (CML4060 – CML4061 d v), 17 km E of Santo Domingo, Los Colorados (CML3026 d v, CML3028 – CML3032 d v, CML3034 d, CML3035

– CML3048 d v, CML 3049 d, CML3050 d v, CML3077 d v, CML3079 d v, CML5195 – CML5959 d v, CML5205 d v); San Luis province, 23 km N of ruta 20, Pampa de las Salinas near to La Botija (CML3515 v, CML3516 d, CML3562 d v); Santiago del Estero province, Buena Vista, 15 km NE to Villa Ojo de Agua on ruta 13 (CML3548 d v), Finca El Duende, Pozo Hondo (CML4126 d v), Pampa de los Guanacos (CML3545 d v), Río Dulce, 5 km E de las Termas (CML4062 d v), Río Saladillo y ruta 9 (CML3543 d v); Tucumán province, San Pedro de Colalao (CML1584 d v, CML1589 d v), Tres Pozos (CML1358 d v).

G. griseoflavus: Argentina. Buenos Aires province, Medanos (GRT017 – GRT023 d v); Catamarca province, Choya, 13 km al NNW de Andalgalá (CML3474 d v); Chubut province, 8 km ESE of Puerto Madryn (CML3927 d v, CML3487 d v); Puerto Madryn (GRT004 d v); Península Valdez (CML1765 d v); Mendoza province, Near to Divisadero Largo (GRT010 – GRT011 d v, GRT012 v, GRT013 – GRT015 d v), 2 km N of Valle Grande (CML3560 d, CML3561 d v), Ñacuñán (CML2133 d v, GRT005 – GRT006 d v, GRT007 d, GRT008 – GRT009 d v), Puesto Punta del Agua (CML3557 – CML3558 d v, CML3559 v); Salta province, 17 km NW of Cachi (CML7109 d v); San Luis province, 12 km N Varela (CML3503 – CML3504 d v), 16 km E Salinas del Bebedero (CML3508 – CML3509 d v,CML3513 – CML3514 d v, CML3566 – CML3567 d v), Rincón de Papagayos, 2 km E of Papagayos (CML3530 d v, CML3533 d v), Papagayos (GRT001 – GRT002 d v), Rió Gómez, 7 km E of San Francisco de Monte de Oro (CML3534 d v), 4 km E of San Francisco de Monte de Oro (CML3538 d v, CML3541 d v), La Calera 12 km NO de Los Araditos (CML3519 d v, CML3521 d v), Parque Nacional Sierra de Las Quijadas (CML3563 – CML3565 d v), Quebrada de López, San Francisco del Monte de Oro (CML3524 d v, CML3527 d v), Villa del Carmen (CUNRC43462 d v); San Juan province, Castaño Nuevo, 9 km NO of Villa Nueva (CML3491 d v, CML3493 d v), Ischigualasto (CML1287 d v, CML1288 v, CML1290 – CML1291 d v, CML1293 d v), Quebrada de las flores, 4 km E and 5 km N Guayamas (CML3568 d v, CML3569 d), Tudcum, Nacedero (CML3498 d v); Tucumán province, Hualinchay (CML1230 d, CML1246 d v).

Appendix B.

Localities of *Graomys* specimens examined, sample size, geographic location and ecoregion.

Localities of Argentina used for this study	Sample size for dorsal view	Sample size for ventral view	Latitude	Longitude	Ecoregion
Laguna La Brea, Jujuy province	1	1	−23.8652	−64.4307	Yungas rainforest
Las Tipas, Parque Biológico, Tucumán province	3	3	−26.6689	−65.4168	Yungas rainforest
35 km S, 5 km E Ingeniero Guillermo Juarez, Puesto Divisadero, Formosa province	3	3	−23.9006	−61.8631	Dry Chaco
Los Colorados, 17 km E of Santo Domingo, Salta province	31	29	−24.2350	−62.5065	Dry Chaco
Cruce entre ruta 81 and 95 7 km N, Formosa province	1	1	−25.2221	−59.7101	Humid Chaco
Estancia Poguazú, Cruce entre ruta 81 and 95 8 km N, Formosa province	1	1	−25.2000	−59.6333	Humid Chaco
Cabeza de Buey, Campo La Peña, Salta province	5	4	−24.7835	−65.0187	Dry Chaco
Río El Guanaco, over ruta provincial 5–32 km NE of La Lumbrera, Salta province	1	1	−25.0041	−64.6866	Dry Chaco
Finca San Javier, 8.5 km SE de Joaquín V. González, Salta province	2	2	−25.2775	−64.1601	Dry Chaco
17 km NW of Cachi, Salta province	1	1	−25.0172	−66.0545	Monte desert
San Pedro de Colalao, Tucumán province	3	2	−26.2418	−65.5066	Yungas rainforest
Tres Pozos, Tucumán province	1	1	−27.0702	−64.9206	Dry Chaco
Hualinchay, Tucumán province	1	1	−26.3047	−65.6557	Yungas rainforest
1 km NE to Cruce between Río Saladillo and ruta nacional 9, Santiago del Estero province	1	1	−28.8697	−63.9723	Dry Chaco

Localities of Argentina used for this study	Sample size for dorsal view	Sample size for ventral view	Latitude	Longitude	Ecoregion
Buena Vista, 15 km NE to Villa Ojo de Agua on ruta 13, Santiago del Estero province	1	1	−29.4590	−63.6001	Dry Chaco
Río Dulce 5 km E of Las Termas, Santiago del Estero province	1	1	−27.5071	−64.8102	Dry Chaco
Finca el Duende, Pozo Hondo, Santiago del Estero province	1	1	−27.1630	−64.4828	Dry Chaco
6 km S, 2 km E of Pampa de los Guanacos, Santiago del Estero province	1	1	−26.2400	−61.8610	Dry Chaco
0.5 km E of ruta 38 over ruta 60, Chumbicha, Catamarca province	5	5	−28.8612	−66.2381	Dry Chaco
Choya, 13 km al NNW de Andalgalá, Catamarca province	1	1	−27.5333	−66.4000	Yungas rainforest
Chamical, La Rioja province	8	7	−30.3671	−66.3472	Dry Chaco
26 km SW of Quimilo, La Rioja province	3	3	−30.0361	−65.5278	Dry Chaco
Guayapa, Patquía, La Rioja province	19	15	−30.0654	−66.8873	Dry Chaco
Agua de la Peña, Ischigualasto, San Juan province	4	5	−30.0989	−67.9104	Monte desert
Castaño Nuevo, 9 km NW of Villa Nueva, San Juan province	2	2	−31.0102	−69.4493	Monte desert
Tudcum, Nacedero, San Juan province	1	1	−30.1979	−69.2771	Monte desert
Quebrada de las flores, 4 km E and 5 km N of Guayamas, San Juan province	2	1	−31.6667	−68.1333	Monte desert
Near to Divisadero Largo, Mendoza province	5	6	−32.9143	−68.8896	Monte desert
Ñacuñán, Mendoza province	6	5	−34.0443	−67.9623	Monte desert
Puesto Punta del Agua 2 km S, Mendoza province	2	4	−35.5774	−68.0665	Monte desert
Valle Grande 2 km N, Mendoza province	2	1	−34.8120	−68.5174	Monte desert
12 km N of Varela, San Luís province	2	2	−34.0105	−66.4524	Monte desert
15 km E of Salinas del Bebedero, San Luís province	6	6	−33.5768	−66.5139	Monte desert
23 km N of ruta 20, Pampa de las Salinas near to La Botija, San Luís province	2	2	−32.1773	−66.5956	Dry Chaco
La Calera 12 km NW of Los Araditos, San Luís province	2	2	−32.8448	−67.1037	Dry Chaco
Quebrada de López, San Francisco del Monte de Oro, San Luís province	2	2	−32.6921	−66.1355	Dry Chaco
Rió Gómez, 7 km E of San Francisco de Monte de Oro, San Luís province	1	1	−32.6097	−66.0548	Dry Chaco
4 km E of San Francisco de Monte de Oro, San Luís province	2	2	−32.6082	−66.0867	Dry Chaco
Rincón de Papagayos, 2 km E of Papagayos, San Luís province	2	2	−32.6908	−64.9645	Dry Chaco
Papagayos, San Luís province	2	2	−32.6939	−64.9827	Dry Chaco
Villa del Carmen, San Luís province	1	1	−32.9531	−65.0526	Dry Chaco
6 km W of Hualtaran, Parque Nacional Sierra de las Quijadas, San Luís province	3	3	−32.4654	−67.0329	Dry Chaco
Cruz del Eje, Córdoba province	13	12	−30.7167	−64.8167	Dry Chaco
Villa de María, Córdoba province	10	11	−29.9062	−63.7026	Dry Chaco
Deán Funes, Córdoba province	3	3	−30.4415	−64.3318	Dry Chaco
10 km N of Santiago Temple, Córdoba province	1	1	−31.3858	−63.4021	Espinal
Yacanto, Córdoba province	2	2	−32.0529	−65.0517	Dry Chaco

Localities of Argentina used for this study	Sample size for dorsal view	Sample size for ventral view	Latitude	Longitude	Ecoregion
Villa Dolores, Córdoba province	1	1	−31.9966	−65.1783	Dry Chaco
Medanos, Buenos Aires province	7	7	−38.8118	−62.6005	Espinal
Península Valdez, Chubut province	1	1	−42.5105	−63.9993	Monte desert
8 km ESE of Puerto Madryn, Chubut province	2	2	−42.8489	−64.9528	Monte desert
Puerto Madryn, Chubut province	1	1	−42.7872	−65.0076	Monte desert

References

Anderson, S., 1997. Mammals of Bolivia, taxonomy and distribution. Bull. Am. Mus. Nat. Hist. 231, 1–652.

Anderson, S., Yates, T.L., 2000. A new genus and species of phyllotine rodent from Bolivia. J. Mamm. 81, 18–36.

Asthon, K.G., Tracy, M.C., de Queiroz, A., 2000. Is Bergmann's rule valid for mammals? Am. Nat. 156, 390–415.

Barraclough, T.G., Vogler, A.P., 2000. Detecting the geographical pattern of speciation from species-level phylogenies. Am. Nat. 155, 419–434.

Bookstein, F.L., 1991. Morphometric Tools for Landmark Data. Cambridge University Press, New York.

Cardini, A., Jansson, A., Elton, S., 2007. A geometric morphometric approach to the study of ecogeographical and clinal variation in Vervet monkeys. J. Biogeogr. 34, 1663–1678.

Catanesi, C.I., Vidal-Rioja, L., Zambelli, A., 2006. Molecular and phylogenetic analysis of mitochondrial control region in Robertsonian karyomorphs of *Graomys griseoflavus* (Rodentia, Sigmodontinae). Mastozool. Neotrop. 13, 21–30.

Catanesi, C.I., Vidal-Rioja, L., Crisci, J.V., Zambelli, A., 2002. Phylogenetic relationships among Robertsonian karyomorphs of *Graomys griseoflavus* (Rodentia, Muridae) by mitochondrial cytochrome b DNA sequencing. Hereditas 136, 130–136.

Colangelo, P., Castiglia, R., Franchini, P., Solano, E., 2010. Pattern of shape variation in the Eastern African gerbils of the genus *Gerbilliscus* (Rodentia, Muridae): environmental correlations and implication for taxonomy and systematics. Mamm. Biol. 75, 302–310.

Coyne, J.A., Orr, H.A., 2004. Speciation. Sinauer Associates, Inc., Sunderland, Massachusetts.

D'Elia, G., 2003. Phylogenetics of Sigmodontinae (Rodentia, Muroidea, Cricetidae), with special reference to the akodont group, and with additional comments on historical biogeography. Cladistics 19, 307–323.

Di Cola, V., Cardozo, G., Lanfri, M., Scavuzzo, C.M., Chiaraviglio, M., 2008. Modelling the distribution of the Boid snakes, *Epicrates cenchria alvarezi* and *Boa constrictor occidentalis* in the Gran Chaco (South America). Amphibia-Reptilia 29, 299–310.

Díaz, M.M., Teta, P., Pardiñas, U.F.J., Barquez, R.M., 2006. Tribu Phyllotini Vorontsov, 1959. In: Barquez, R.M., Díaz, M.M., Ojeda, R.A., 2006. Mamíferos de Argentina. Sistemática y distribución. Sarem, Tucumán, Argentina.

Díaz, M.M., 1999. Los mamíferos de Jujuy: sistemática, distribución y ecología. PhD dissert. Facultad de Ciencias Naturales e Instituto Miguel Lillo, Universidad Nacional de Tucumán. 640 pp.

Díaz, M.M., Barquez, R.M., 2007. The wild mammals of Jujuy province: systematics and distribution. In: Kelt, D.A., Lessa, E.P., Salazar-Bravo, J., Patton, J.L. (Eds.), The Quintessential Naturalist: Honoring the Life and Legacy of Oliver P. Pearson, vol. 134. Univ. Calif. Publ. Zool., pp. 417–578.

Elith, J., Graham, C.H., Anderson, R.P., Dudik, M., Ferrier, S., Guisan, A., Hijmans, R.J., Huettmann, F., Leathwick, J.R., Lehmann, A., Li, J., Lohmann, L.G., Loiselle, B.A., Manion, G., Moritz, C., Nakamura, M., Nakazawa, Y., Overton, J., Peterson, McC., Phillips, A.T., Richardson, S.J., Scachetti-Pereira, K., Schapire, R., Soberón, R.E., Williams, J., Wisz, S., Zimmermann, M.S., 2006. Novel methods improve prediction of species' distributions from occurrence data. Ecography 29, 129–151.

Fadda, C., Corti, M., 2001. Three-dimensional geometric morphometrics of *Arvicanthis*: implications for systematics and taxonomy. J. Zool. Syst. Evol. Res. 39, 235–245.

Ferro, L.I., Martínez, J.J., 2009. Molecular and morphometric evidences validate a Chacoan species of the grey leaf-eared mice genus *Graomys* (Rodentia: Cricetidae: Sigmodontinae). Mammalia 73, 265–271.

Fu, Y.X., 1997. Statistical test of neutrality of mutations against population growth, hitchhiking and background selection. Genetics 147, 915–925.

García, A.A., 2003. Reevaluación de los niveles de género y especie asignados al filotino *Andalgalomys* (Muridae: Sigmodontinae): Evidencias citogenéticas y moleculares. PhD dissert. Universidad Nacional de San Luís, San Luís, Argentina.

García, A.A., Walker, L., 2004. Fusiones céntricas independientes en poblaciones de *Graomys griseoflavus* (Rodentia: Sigmodontinae). JAM 9, 85.

González-José, R., Bortolini, M.C., Santos, F.R., Bonatto, S.L., 2008. The peopling of America: craniofacial shape variation on a continental scale and its interpretation from an interdisciplinary view. Am. J. Phys. Anthropol. 137, 175–187.

Hammer, Ø., Harper, D.A., Ryan, P.D., 2001. PAST: paleontological statistics software package for education and data analysis. Palaeontol. Electron. 4, 1.

Hernandez, P.A., Graham, C.H., Master, L.L., Albert, D.L., 2006. The effect of sample size and species characteristics on performance of different species distribution modeling methods. Ecography 29, 773–785.

Hijmans, R.J., Cameron, S., Parra, J., Jones, P., Jarvis, A., 2005. Very high resolution interpolated climate surfaces for global land areas. Int. J. Climatol. 25, 1965–1978.

Hingst-Zaher, E., Marcus, L.F., Cerqueira, R., 2000. Application of geometric morphometrics to the study of postnatal size and shape changes in the skull of *Calomys expulsus*. Hystrix 11, 99–113.

InfoStat, 2008. InfoStat version 2008. Grupo InfoStat, FCA. Universidad Nacional de Córdoba, Argentina.

Kozak, K.H., Graham, C.H., Wiens, J.J., 2008. Integrating GIS-based environmental data into evolutionary biology. Trends Ecol. Evol. 23, 141–148.

Lanzone, C., Novillo, A., Suárez, N.S., Ojeda, R.A., 2007. Cytogenetics and redescription of *Graomys* (Sigmodontinae) from Chumbicha, Argentina. Mastozool. Neotrop. 14, 249–255.

Lockwood, C.A., Kimbel, W.H., Lynch, J.M., 2004. Morphometrics and hominoid phylogeny: support for a chimpanzee-human clade and differentiation among great ape subspecies. Proc. Natl. Acad. Sci. U.S.A. 101, 4356–4360.

Macholán, M., Mikula, O., Vohralík, V., 2008. Geographic phenetic variation of two eastern-Mediterranean non-commensal mouse species. *Mus macedonicus* and *M. cypriacus* (Rodentia: Muridae) based on traditional and geometric approaches to morphometrics. Zool. Anz. 247, 67–80.

Macholán, M., 2008. The mouse skull as a source of morphometric data for phylogeny inference. Zool. Anz. 247, 315–327.

Mantel, N.A., 1967. The detection of disease clustering and a generalized regression approach. Cancer Res. 27, 209–220.

Martínez, J.J., Krapovickas, J.M., Theiler, G.R., 2010a. Morphometrics of *Graomys* (Rodentia; Cricetidae) from Central-Western Argentina. Mamm. Biol. 75, 180–185.

Martínez, J.J., Gonzalez-Ittig, R.E., Theiler, G.R., Ojeda, R., Lanzone, C., Ojeda, A., Gardenal, C.N., 2010b. Patterns of speciation in two sibling species of *Graomys* (Rodentia, Cricetidae) based on mtDNA sequences. J. Zool. Syst. Evol. Res. 48, 159–166.

Meiri, S., Dayan, T., 2003. On the validity of Bergmann's rule. J. Biogeogr. 30, 331–351.

Monteiro, L.R., Duarte, L.C., Dos Reis, S.F., 2003. Environmental correlates of geographical variation in skull and mandible shape of the punare rat *Thrichomys apereoides* (Rodentia: Echimydae). J. Zool. 261, 47–57.

Myers, P., 1989. A preliminary revision of the *varius* group of *Akodon* (*A. dayi. dolores, molinae, neocenus, simulator, toba and varius*). In: Redford, K., Eisenberg, J.F. (Eds.), Advances in Neotropical Mammalogy. Sandhill Crane Press, Gainesville, Florida, pp. 5–54.

Peakall, R., Smouse, P.E., 2006. GENALEX 6: genetic analysis in Excel. Population genetic software for teaching and research. Mol. Ecol. Notes 6, 288–295.

Pearson, O.P., Patton, J.L., 1976. Relationships among South American phyllotine rodents based on chromosome analysis. J. Mamm. 57, 339–350.

Pearson, R.G., Raxworthy, C.J., Nakamura, M., Peterson, A.T., 2007. Predicting species distributions from small numbers of occurrence records: a test case using cryptic geckos in Madagascar. J. Biogeogr. 34, 102–117.

Pearson, R.G., Thuiller, W., Araújo, M.B., Martínez-Meyer, E., Brotons, L., McClean, C., Miles, L., Segurado, P., Dawson, T.P., Lees, D.C., 2006. Model-based uncertainty in species range prediction. J. Biogeogr. 33, 1704–1711.

Phillips, S.J., Anderson, R.P., Schapire, R.E., 2006. Maximum entropy modeling of species geographic distributions. Ecol. Model. 190, 231–259.

Phillips, S.J., Dudík, M., Schapire, R.E., 2004. A maximum entropy approach to species distribution modelling. In: Proceedings of the 21st International Conference on Machine Learning. ACM Press, New York, pp. 655–662.

Piras, P., Marcolini, F., Raia, P., Curcio, M., Kotsakis, T., 2010. Ecophenotypic variation and phylogenetic inheritance in first lower molar shape of extant Italian populations of *Microtus* (*Terricola*) *savii* (Rodentia). Biol. J. Linn. Soc. 99, 632–647.

Ramirez, P.B., Bickham, J.W., Braun, J.K., Mares, M.A., 2001. Geographic variation in genome size of *Graomys griseoflavus* (Rodentia: Muridae). J. Mamm. 82, 102–108.

Rissler, L.J., Apodaca, J.J., 2007. Adding more ecology into species delimitation: ecological niche models and phylogeography help define cryptic species in the black salamander (*Aneides flavipunctatus*). Syst. Biol. 56, 924–942.

Rissler, L.J., Hijmans, R.J., Graham, C.H., Moritz, C., Wake, D.B., 2006. Phylogeographic lineages and species comparisons in conservation analysis: a case study of California herpetofauna. Am. Nat. 167, 655–666.

Rogers, A.R., Harpending, H., 1992. Population growth makes waves in the distribution of pairwise genetic differences. Mol. Biol. Evol. 9, 552–569.

Rohlf, F.J., 2005a. tpsDig2. Department of Ecology and Evolution, State University of New York at Stony Brook.

Rohlf, F.J., 2005b. tpsPLS. Department of Ecology and Evolution, State University of New York at Stony Brook.

Rohlf, F.J., 2005c. tpsRegr. Department of Ecology and Evolution, State University of New York at Stony Brook.

Rohlf, F.J., 2005d. tpsRelw, relative warps analysis. Department of Ecology and Evolution, State University of New York at Stony Brook.

Rohlf, F.J., 2005e. tpsSmall. Department of Ecology and Evolution, State University of New York at Stony Brook.

Rohlf, F.J., Corti, M., 2000. Use of two-block partial least-squares to study covariation in shape. Syst. Biol. 49, 740–753.

Rohlf, F.J., Slice, D.E., 1990. Extensions of the Procrustes method for the optimal superimpositions of landmarks. Syst. Zool. 39, 40–59.

Sheets, H.D., 2001a. IMP CVAGen6. Buffalo, Canisius College. State University of New York.

Sheets, H.D., 2001b. IMP Regress6. Buffalo, Canisius College. State University of New York.

Stockman, A.K., Bond, J.E., 2007. Delimiting cohesion species: extreme population structuring and the role of ecological interchangeability. Mol. Ecol. 16, 3374–3392.

Stockman, A.K., Danell, R.M., Bond, J.E., 2008. D-NOLV: a program to simulate overlap between two niche-based distribution models. Mol. Ecol. Resources 8, 290–294.

Suárez, S.N., Lanzone, C., Ojeda, A., Rodríguez, D., 2006. Estudios citogenéticos en *Graomys griseoflavus* (Rodentia, Cricetidae, Sigmodontinae) en las provincias de Mendoza y Catamarca. BAG 17, 117.

Taylor, P.J., Kumirai, A., Contrafatto, G., 2004. Geometric morphometric analysis of adaptive cranial evolution in southern African laminate-toothed rats (Family: Muridae, Tribe: Otomyni). Durban Mus. Novit. 29, 110–122.

Theiler, G.R., 1997. Patrones de evolución en *Graomys griseoflavus* (Rodentia, Muridae). Un caso de especiación rápida. PhD dissert. Facultad de Ciencias Exactas, Físicas y Naturales; Universidad Nacional de Córdoba; Argentina.

Theiler, G.R., Blanco, A., 1996a. Patterns of evolution in *Graomys griseoflavus* (Rodentia, Muridae). III. Olfactory discrimination as a premating isolation mechanism between cytotypes. J. Exp. Zool. 274, 346–350.

Theiler, G.R., Blanco, A., 1996b. Patterns of evolution in *Graomys griseoflavus* (Rodentia, Muridae). II. Reproductive isolation between cytotypes. J. Mamm. 77, 776–784.

Theiler, G.R., Gardenal, C.N., 1994. Patterns of evolution in *Graomys griseoflavus* (Rodentia, Cricetidae). I. Protein polymorphism in populations with different chromosome number. Hereditas 120, 225–229.

Theiler, G.R., Gardenal, C.N., Blanco, A., 1999. Patterns of evolution in *Graomys griseoflavus* (Rodentia, Muridae). IV. A case of rapid speciation. J. Evol. Biol. 12, 970–979.

Thomas, O., 1902. On mammals collected at Cruz del Eje, Central Cordoba, by Mr. P. O. Simmons. Ann. Mag. Nat. Hist. 7, 237–245.

Thomas, O., 1926. The Spedan Lewis South American exploration. II. On mammals collected in the Tarija department, Southern Bolivia. Ann. Mag. Nat. Hist. Ibid., 318–328.

Tiranti, S.I., 1998. Cytogenetics of *Graomys griseoflavus* (Rodentia: Sigmodontinae) in Central Argentina. Z. Säugetierk. 63, 32–36.

Wainberg, R.L., Fronza, T.G., 1974. Autosomic polymorphism in *Phyllotis griseoflavus griseoflavus* Waterhouse, 1837 (Rodentia, Cricetidae). Boll. Zool. 41, 19–24.

Webster, D.B., 1962. A function of the enlarged of the middle-ear cavities of the Kangaroo rat, *Dipodomys*. Physiol. Zool. 35, 248–255.

Webster, D.B., 1966. Ear structure and function in modern mammals. Am. Zool. 6, 451–466.

Webster, D.B., Webster, M., 1980. Morphological adaptations of the ear in the rodent Family Heteromyidae. Am. Zool. 20, 247–254.

Wiens, J.J., 2004. Speciation and ecology revisited: phylogenetic niche conservatism and the origin of species. Evolution 58, 193–197.

Zambelli, A., Vidal-Rioja, L., Wainberg, R., 1994. Cytogenetic analysis of autosomal polymorphism in *Graomys griseoflavus* (Rodentia, Cricetidae). Z. Säugetierk. 59, 14–20.

Zelditch, M.L., Swiderski, D.L., Sheets, H.D., Fink, W.L., 2004. Geometric Morphometrics for Biologist: A Primer. Elsevier Academic Press, San Diego.